Estuarine, Coastal and Shelf Science 207 (2018) 269–282

Contents lists available at ScienceDirect

Estuarine, Coastal and Shelf Science

journal homepage: www.elsevier.com/locate/ecss

Fluxes of dissolved organic carbon and nutrients via submarine groundwater discharge into subtropical Sansha Bay, China

Guizhi Wang[a,b,c,*], Aiqin Han[d,**], Liwen Chen[c], Ehui Tan[c], Hui Lin[d]

[a] State Key Laboratory of Marine Environmental Science, Xiamen University, Xiamen, China
[b] Fujian Provincial Key Laboratory for Coastal Ecology and Environmental Studies, Xiamen University, Xiamen, China
[c] College of Ocean and Earth Sciences, Xiamen University, Xiamen, China
[d] Third Institute of Oceanography, State Oceanic Administration, Xiamen, China

A B S T R A C T

To evaluate the role that submarine groundwater discharge (SGD) plays in the carbon and nutrient budgets in subtropical Sansha Bay, southeastern China, radium isotopes were used as SGD tracers and investigated in the bay and surrounding groundwater. In general, the activity of radium isotopes (^{223,224,226,228}Ra) decreased from the bay head to the outlet that connects with the East China Sea. Based on the ratio of ^{224}Ra and ^{228}Ra, the water age was estimated to be 5.49 ± 3.64 and 1.50 ± 0.83 days in winter and summer, respectively. A three end-member mixing model and a box model were set up based on the mass balance of ^{226}Ra and salinity to quantify SGD. The flux of SGD was calculated to be 9.33 ± 8.17 × 10^5 m^3 d^{-1} (3.8 ± 3.4 × 10^{-3} m^3 m^{-2} d^{-1}) in winter and 4.89 ± 3.35 × 10^6 m^3 d^{-1} (2.0 ± 1.4 × 10^{-2} m^3 m^{-2} d^{-1}) in summer, which were at least a few times less than the concomitant river discharge into the bay. In groundwater, an enrichment of dissolved inorganic nitrogen, phosphorus, and organic carbon was associated with relatively high activities of ^{226}Ra. The SGD-associated nutrient flux was 1.99 ± 1.74–95.0 ± 83.2 μmol m^{-2} d^{-1} in winter and 0–0.89 ± 0.55 mmol m^{-2} d^{-1} in summer of phosphate, 6.76 ± 5.92–7.21 ± 6.32 mmol m^{-2} d^{-1} in winter and 66.2 ± 40.8–93.6 ± 57.7 mmol m^{-2} d^{-1} in summer of dissolved inorganic nitrogen, and 1.20 ± 1.05–1.74 ± 1.52 mmol m^{-2} d^{-1} in winter and 5.93 ± 4.06–8.22 ± 5.63 mmol m^{-2} d^{-1} in summer of silicate. The flux of dissolved organic carbon via SGD was 0.17 ± 0.15–0.33 ± 0.29 mmol m^{-2} d^{-1} in winter and 1.31 ± 0.81–2.94 ± 1.81 mmol m^{-2} d^{-1} in summer. The flux of N carried by SGD into Sansha Bay was comparable to the estuarine flux in winter, while was an order of magnitude greater than the estuarine flux in summer. The minimum flux of silicate via SGD was about half as much as the estuarine flux in summer, while was an order of magnitude smaller than the estuarine flux in winter. The minimum SGD-associated P flux was at least two orders of magnitude smaller than the estuarine flux in both seasons. Therefore, SGD on embayment scale is an important pathway for nitrogen from land to sea. These great SGD-associated nutrient fluxes may contribute to eutrophication and hypoxia in such stratified embayment.

1. Introduction

Submarine groundwater discharge (SGD) is defined as the flow of water from the seabed to the coastal ocean at scales ranging from meters to kilometers (Moore, 2010). It has been recognized and quantified as an important pathway for terrestrially derived materials into the coastal zone, with fluxes of carbon, nutrients, and metals comparable to local/regional riverine fluxes (Cai et al., 2003; Gu et al., 2012; Kim et al., 2011; Moore, 2010; Porubsky et al., 2014; Wang et al., 2015). SGD studies have been carried out on embayment and shelf scales mostly in terms of fluxes of nutrients and their impacts on marine ecosystems (Kim et al., 2005; Rodellas et al., 2015; Tait et al., 2014; Umezawa et al., 2002) but less in respect of carbon fluxes (Liu et al., 2012; Liu et al., 2014; Stewart et al., 2015). However, great spatial variability in SGD makes studies in more latitudes and ecosystems warranted.

As a significant carbon and nutrient source, as well as characterized by relatively low pH and dissolved oxygen, SGD may exert great biogeochemical and environmental impacts on coastal ecosystems. It has been estimated that up to 93% of the SGD-associated flux of dissolved inorganic nitrogen (DIN, including nitrate, nitrite, and ammonium) is utilized by primary production in embayments (Kim et al., 2011).

* Corresponding author. State Key Laboratory of Marine Environmental Science, Xiamen University, Xiamen, 361102, China.
** Corresponding author. Third Institute of Oceanography, State Oceanic Administration, Xiamen, China.
E-mail address: gzhwang@xmu.edu.cn (G. Wang).

https://doi.org/10.1016/j.ecss.2018.04.018
Received 24 July 2017; Received in revised form 9 April 2018; Accepted 16 April 2018
Available online 17 April 2018
0272-7714/

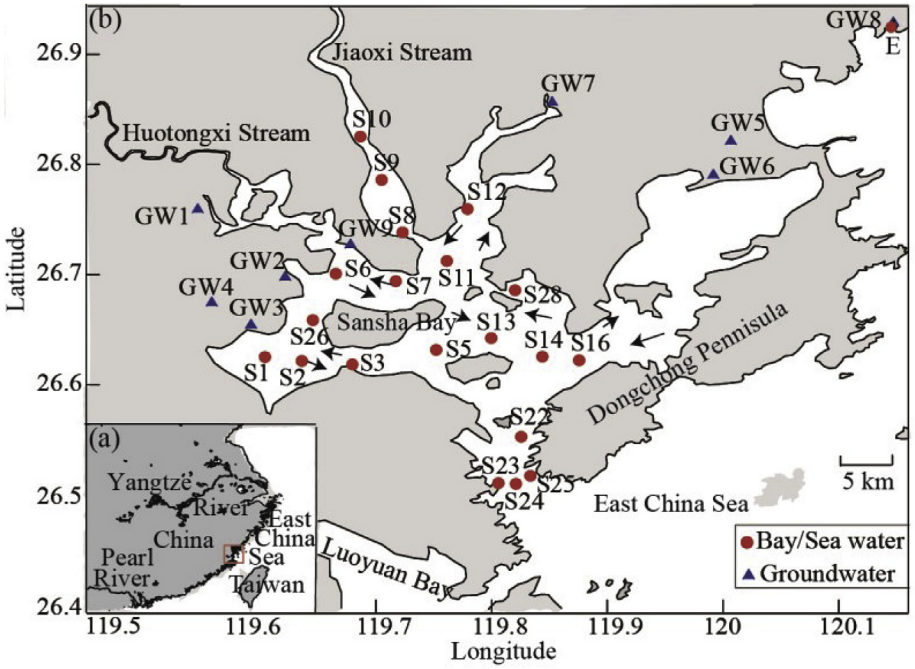

Fig. 1. Study area (a) and sampling stations in Sansha Bay and East China Sea and of nearby groundwater (b). The arrows represent tidal currents from Shen et al. (2014).

Eutrophication and even algal blooms have been reported to be induced by SGD (Hwang et al., 2005; Lee and Kim, 2007; Rocha et al., 2015). Coastal acidification and hypoxia have been shown to be linked with SGD (McCoy et al., 2011; Santos et al., 2011; Wang et al., 2014a). Therefore, SGD and associated material fluxes are factors that need to be taken into consideration in biogeochemical studies of any coastal system.

Naturally occurring radium isotopes are good tracers of SGD because they are highly enriched in groundwater compared to those in rivers and coastal waters and show strong signals in surface waters once discharged via SGD (Moore, 2010). The long-lived Ra, ^{226}Ra (half life = 1600 yr) and ^{228}Ra (half life = 5.75 yr), are useful in estimating SGD fluxes into coastal waters (Kim et al., 2005; Krest et al., 1999; Krest et al., 2000; Wang et al., 2015), while the short-lived Ra, ^{223}Ra (half life = 11.4 d) and ^{224}Ra (half life = 3.66 d), serve well in estimating mixing rates and residence time of coastal waters (Moore, 2000a; Moore, 2000b; Moore et al., 2006).

Sansha Bay is a subtropical embayment, located on the southeast coast of China (Fig. 1). It is a natural spawning ground for large yellow croakers. With economic developments and increasing human perturbations around the area, Sansha Bay has experienced nutrient pollution in most areas (Zhu et al., 2013). The water quality in the bay has degraded in the past two decades (Yu et al., 2014), mainly due to developments in aquaculture in the bay and agriculture around the bay (Wang et al., 2011). SGD, as a potentially important land-based solute source, however, has never been quantified and evaluated in this bay. In this study we aimed to quantify SGD and associated fluxes of dissolved organic carbon (DOC) and nutrients into Sansha Bay. Radium isotopes were utilized as SGD tracers in this study.

2. Materials and methods

2.1. Study area

Sansha Bay, located on the northeast coast of Fujian Province, China, is a semi-enclosed bay with an outlet about 2.9 km wide to the East China Sea (ECS) (Fig. 1). Waves can hardly directly influence the bay due to the narrow outlet (Ye et al., 2007). The bay has a surface water area of about 675 km^2 (Lin et al., 2016a) and a tortuous coast line of 553 km (Lin, 2014). It is surrounded by hills where medium acidic volcanic rocks outcrop (Yan and Cao, 1997). Quaternary deposits accumulate in the piedmonts along the coast of the bay (Wu, 2011). Meteoric groundwater in this area includes interstitial waters in the high-permeability Quaternary deposits and extensive bedrock fissure waters that are spatially inhomogeneous (Wu, 2011). No hydraulic gradients and groundwater discharge along the coast of Sansha Bay are available so far from literature. The average annual precipitation in this area is 1700 mm, mostly in March–September (Fig. 2) (Xiong et al., 2015). Strong semi-diurnal tides dominate in the bay, with a tidal period of 12 h 24 min and an average tidal range of greater than 5 m (Lin, 2014). The tidal prism is 2.68 × 10^9 m^3 (Wang et al., 2011). The pattern of tidal currents is similar in winter and summer (Fig. 1), with periodic alternating currents along the main water channels (Shen et al., 2014). The water depth in the bay varies from a few meters to 90 m (Cai, 2007). Seasonal monsoon prevails in this area, with southwest winds in summer and northeast winds in winter. Influenced by the monsoon winds, the ambient ECS offshore water is a mixture of the Minzhe Coastal Current (MCC) and Taiwan Warm Current (TWC), the proportions of which vary with season. MCC predominates under the northeast monsoon in winter and TWC prevails in summer (Xu and Xu, 2013). The mixed layer depth in the bay is deeper in winter than in summer due to stronger winter monsoon (Lin et al., 2016a). A few mountainous rivers flow into Sansha Bay, with two streams predominant, Jiaoxi Stream and Huotongxi Stream (Chen et al., 2014; Xu et al., 2014). Jiaoxi Stream has a watershed of 5549 km^2 with an average annual discharge of 6.97 × 10^{10} m^3 (Huang and Ding, 2014). The watershed of Huotongxi Stream is 2244 km^2 and its average annual water discharge is 2.73 × 10^9 m^3 (Li et al., 2014). The farmland around Sansha Bay is 5.28 × 10^4 ha and the sediments due to farmland soil loss into Sansha Bay have been estimated to be 1.23 × 10^8 kg, carrying N and P into the bay (Li et al., 2009). The sediments in the bay are mainly composed of silty clay and clayey silts, which originate mainly from MCC and are subsequently carried inside the bay by tidal currents, and high-permeability sands are located nearshore, which originate from surface runoffs and coastal erosion (Yan and Cao, 1997). Aquaculture in Sansha Bay has developed quickly in the last few decades. By 2009

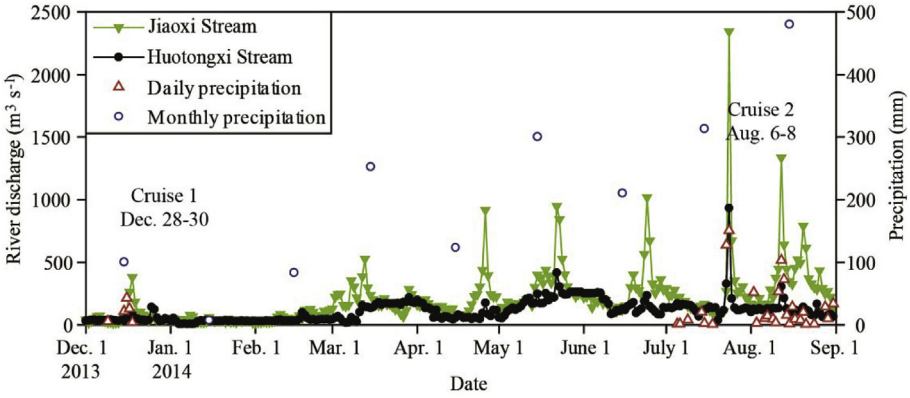

Fig. 2. The daily average river discharge of Jiaoxi Stream and Huotongxi Stream and precipitation in this area during the period of Dec. 1, 2013 to Aug. 31, 2014. The daily average discharge was calculated from discharge data at hydrological stations Baita and Yangzhongban, which are located downstream of Jiaoxi Stream and Huotongxi Stream, respectively, provided by the Bureau of Hydrology, Ministry of Water Resources, China at the website http://xxfb.hydroinfo.gov.cn. The daily precipitation was recorded at the hydrological station Baita provided by China Meteorological Data Service Center at the website http://data.cma.cn. The monthly precipitation was provided in Xiong et al. (2014, 2015).

there were 2.2×10^5 cages in the bay with 1×10^4 fish in each cage (Zhu et al., 2013). Habitats in the bay degraded from 1991 to 2012, mainly due to anthropogenic disturbance that were mostly caused by local agriculture and aquaculture developments, with spatial and temporal heterogeneity (Yu et al., 2014). Hypoxia has been observed since the beginning of this century and is related to aquaculture development in the bay (Wang et al., 2014b).

2.2. Sampling and measurements

Large volume dissolved radium samples (about 40 l) were collected from the surface using a plastic barrel and from depth using Niskin bottles in the bay (Fig. 1) onboard R/V Minningyu F622 in two cruises, one during December 28–30, 2013 when the total river discharge ranged 70–95 $m^3 s^{-1}$ and the other during August 6–8, 2014 when the total river discharge was 289–401 $m^3 s^{-1}$ (Fig. 2). Surface sampling stations were the same in both seasons, while bottom sampling stations were different. In the winter cruise water samples at the bottom depth were collected at stations S2, S26, S5, S7, and S28. In the summer cruise a radium profile, including bottom depth, was sampled at Station 14. Profiles of temperature and salinity were measured using a conductivity-temperature-depth (CTD) system (Ocean Seven 316 Plus, IDRONAUT S.R.L. Co., Italy). Nutrient samples were collected using Niskin bottles at the same time in the bay in both seasons. But only nutrient data at the stream stations are reported in this paper. DOC samples were not collected in the bay during the cruises. Water samples for radium were passed through a 1 μm cartridge filter followed by a MnO_2-impregnated acrylic fiber (Mn-fiber) column to extract radium at a flow rate of less than 500 ml min^{-1}. The extraction efficiency of the Mn-fiber was greater than 95%, as verified using two Mn-fiber columns connected in series (Kelly and Moran, 2002). The Mn-fiber was rinsed with deionized water and partially dried with a stream of air, then ^{223}Ra and ^{224}Ra were measured with a radium delayed coincidence counter (RaDeCC) as described in Moore and Arnold (1996). The error for the short-lived Ra measurements is less than 5%. After the ^{223}Ra and ^{224}Ra measurements were done, the Mn-fibers were leached with 1 M solutions of hydroxylamine hydrochloride and 1 M HCl to release ^{228}Ra and ^{226}Ra with efficiency of 93% or more (Moore et al., 1985), which were then co-precipitated with $BaSO_4$. The precipitate was concentrated by centrifuging and aged for 3 weeks before being measured in a germanium gamma detector with a 1-cm diameter well (Canberra GCW4022) for ^{226}Ra and ^{228}Ra as described in Moore (1984). The error for the long-lived Ra measurements is less than 7%. To ensure our data quality, our lab participated in the Ra Asian inter-comparison experiment and our results were close to the averages within 1 standard deviation (Du et al., 2013). Total suspended matter (TSM) was collected on pre-weighed and pre-combusted 142-mm-diameter GF/F filter (pore size of 0.7 μm) and weighed after drying. Particulate ^{224}Ra and ^{228}Th samples were also collected on these filters. After returning to the laboratory within 8 h, the sample was partially dried by a stream of air and measured using a RaDeCC system with the sample chamber modified by Cai et al. (2012) for activities of ^{224}Ra and ^{228}Th on these particles. Nutrient samples were filtered with 0.45 μm cellulose acetate membranes and poisoned with 1–2‰ chloroform. One filtrate for ammonium and silicate was preserved at 4 °C, and one for nitrate, nitrite, and phosphate was frozen and kept at −20 °C. Nitrate, nitrite, silicate, and phosphate were measured with an AA3 Auto-Analyzer (Bran-Luebbe, GmbH), while ammonium was measured using a spectrophotometer (Xingsha Instrument, 722) following the same procedures in Yan et al. (2012). The analytical precision was better than 1% for nitrate and nitrite, 2% for phosphate, and 2.8% for ammonium and silicate. The detection limit was 0.03 μM for nitrate and nitrite, 0.03 μM for phosphate, 0.5 μM for ammonium, and 0.05 μM for silicate.

Groundwater samples were collected using a peristaltic pump (DRIVE MFLEX L/S) from domestic wells around the bay (Fig. 1). Stations GW1-4 were sampled in the winter and summer (Table 1), while stations GW 5–7 were sampled only in the summer of 2014 and stations GW8-9 were sampled only in the winter of 2013. Wells were purged for about 30 min before sampling. Dissolved radium was extracted and measured in the same way as the bay water samples. DOC samples were collected after passing through precombusted 0.7 μm GF/F filters in precombusted EPA vials and stored at −20 °C. This practical definition of DOC may include bacteria smaller than 0.7 μm (Verdugo et al., 2004). DOC was measured using a Shimadzu TOC-V analyzer in the same way as TOC measurements detailed in Wu et al. (2015). The analytical precision was ± 0.8 μM. Nutrient samples were processed and measured in the same way as the bay water samples. One DOC sample was collected in the surface water on the East China Sea coast at Station E (120.1469 °E, 26.9296 °N) during the groundwater sampling period in the winter of 2013 to determine the DOC level of the ambient sea water (Fig. 1). The DOC sample was processed and measured in the same way as the groundwater samples. Salinity was measured using a WTW multi-parameter sensor.

3. Results

3.1. Hydrography in Sansha Bay

In winter surface temperature and salinity in Sansha Bay were lower near the Jiaoxi Stream and Huotongxi Stream and increased toward the bay outlet due to mixing with the ECS water (Fig. 3a and b). Surface temperature varied from 12.3 to 15.2 °C and surface salinity fell in the range of 20.3–29.1. At stations in the Jiaoxi Stream the temperature was between 13.2 and 14.6 °C and the salinity ranged from 15.5 to 20.6. In summer surface temperature was higher near the coastline and decreased toward the bay outlet, while surface salinity followed the same pattern as in winter (Fig. 4a and b). Surface temperature ranged from 27.3 to 30.9 °C and surface salinity increased from 20 near the streams

Table 1
Activities of dissolved radium isotopes, temperature (T) and salinity (S) in Sansha Bay in winter (December 2013) and summer (August 2014).

Station[a]	Latitude	Longitude	T	S	^{223}Ra	^{224}Ra	^{226}Ra	^{228}Ra
	°N	°E	°C		dpm 100 L^{-1}			
Winter (December 2013)								
S1	26.6251	119.6039	12.3	25.2	4.93 ± 0.72	45.3 ± 1.9	27.5 ± 0.7	114.5 ± 2.2
S2	26.6215	119.6358	12.9	26.3	3.66 ± 0.51	35.4 ± 1.6	26.3 ± 0.6	112.8 ± 2.1
S2_B	26.6215	119.6358	12.5	26.1	3.75 ± 0.55	42.3 ± 1.8	35.9 ± 0.7	154.0 ± 2.4
S26	26.6585	119.6453	13.2	23.9	3.12 ± 0.32	47.8 ± 1.2	27.3 ± 0.7	123.4 ± 2.4
S26_B	26.6585	119.6453	14.1	26.4	3.08 ± 0.47	32.5 ± 1.7	31.9 ± 1.5	127.0 ± 4.2
S6	26.7009	119.6651	13.3	20.3	1.45 ± 0.21	16.7 ± 0.8	11.5 ± 0.3	37.5 ± 0.9
S7	26.6941	119.7172	14.5	23.3	2.69 ± 0.46	45.8 ± 2.1	29.5 ± 0.7	126.9 ± 2.5
S7_B	26.6941	119.7172	14.7	25.9	3.83 ± 0.56	46.8 ± 2.3	33.4 ± 1.0	130.6 ± 3.4
S5	26.6315	119.7521	14.6	27.3	1.28 ± 0.19	17.4 ± 0.8	24.7 ± 0.8	101.2 ± 2.3
S5_B	26.6315	119.7521	14.6	28.2	2.02 ± 0.29	21.1 ± 1.1	29.4 ± 1.5	112.2 ± 4.4
S3	26.6183	119.6794	14.2	27.5	1.53 ± 0.20	13.0 ± 0.8	13.0 ± 0.5	47.2 ± 1.3
S13	26.6422	119.7996	14.5	28.3	1.07 ± 0.22	10.8 ± 0.9	21.0 ± 0.6	87.3 ± 2.1
S28	26.6859	119.8202	15	27.3	2.07 ± 0.27	18.1 ± 1.1	22.2 ± 0.9	88.3 ± 2.5
S28_B	26.6859	119.8202	14.9	27.3	2.16 ± 0.33	24.8 ± 1.5	31.3 ± 1.7	119.4 ± 3.8
S12	26.7595	119.7791	13	25.5	0.96 ± 0.17	13.1 ± 0.7	12.9 ± 0.4	47.0 ± 1.1
S11	26.7124	119.7613	15.2	23.7	2.42 ± 0.43	45.0 ± 2.0	24.5 ± 0.7	95.2 ± 2.4
S8	26.7383	119.7231	14.6	20.6	3.19 ± 0.51	51.0 ± 2.0	26.1 ± 0.7	103.2 ± 2.9
S9	26.7859	119.7050	13.9	19.5	3.63 ± 0.70	71.7 ± 3.5	26.7 ± 0.6	103.2 ± 2.3
S10	26.8255	119.6863	13.2	15.5	1.90 ± 0.39	53.2 ± 2.1	20.5 ± 0.7	72.8 ± 2.1
S23	26.5108	119.8058	15.1	28.7	1.45 ± 0.24	12.8 ± 1.0	21.2 ± 0.9	82.7 ± 2.7
S24	26.5102	119.8209	15.2	29.1	1.67 ± 0.24	13.1 ± 1.0	24.0 ± 0.5	90.8 ± 1.8
S25	26.5174	119.8334	14.9	29	1.78 ± 0.22	12.5 ± 0.7	21.8 ± 0.8	86.6 ± 2.5
S22	26.5528	119.8255	15	28.3	1.43 ± 0.24	11.4 ± 0.9	21.7 ± 0.6	91.1 ± 2.5
S16	26.6221	119.8758	15	28.2	1.36 ± 0.19	15.5 ± 0.9	23.2 ± 0.6	97.1 ± 2.3
S14	26.6254	119.8437	15	28	0.84 ± 0.19	14.8 ± 0.9	21.0 ± 0.6	86.0 ± 2.0
Summer (August 2014)								
S23	26.5138	119.8059	27.3	30.9	1.69 ± 0.34	22.5 ± 0.8	15.9 ± 0.5	45.5 ± 1.2
S24	26.5124	119.8202	28.2	29.6	1.30 ± 0.27	22.2 ± 0.7	18.2 ± 0.5	49.3 ± 1.6
S25	26.5184	119.8347	27.9	30.9	1.39 ± 0.17	20.0 ± 1.2	14.9 ± 0.5	41.5 ± 1.2
S22	26.5535	119.826	28.1	29.6	1.09 ± 0.18	25.0 ± 1.5	18.1 ± 0.6	52.0 ± 1.6
S16	26.6207	119.8743	28.8	27.8	2.07 ± 0.38	37.5 ± 1.7	21.1 ± 0.5	64.3 ± 1.5
S2	26.6206	119.6369	29.4	26.5	1.89 ± 0.40	51.2 ± 1.6	25.4 ± 0.7	84.5 ± 1.9
S1	26.6252	119.6053	30.3	24.9	2.83 ± 0.51	76.4 ± 1.8	33.6 ± 1.0	95.3 ± 2.4
S26	26.6586	119.6451	30	22.5	2.92 ± 0.50	59.4 ± 1.6	28.7 ± 0.8	94.7 ± 2.1
S6	26.7005	119.6651	29.3	20	2.16 ± 0.44	67.0 ± 1.8	28.9 ± 0.6	90.0 ± 1.6
S7	26.6944	119.7181	29.1	23.6	2.74 ± 0.41	55.3 ± 1.5	25.2 ± 0.6	80.6 ± 1.8
S14	26.6265	119.8403	29.4	26.4	1.88 ± 0.24	42.2 ± 1.2	22.6 ± 0.6	65.8 ± 1.9
S14_5m	26.6265	119.8403	27.9	28.9	1.63 ± 0.26	37.5 ± 2.2	20.8 ± 0.6	63.7 ± 1.4
S14_11m	26.6265	119.8403	28.5	29.8	1.24 ± 0.25	29.7 ± 1.7	21.8 ± 0.8	66.3 ± 2.4
S14_41m	26.6265	119.8403	26.9	31.1	1.28 ± 0.22	16.7 ± 1.1	20.2 ± 0.6	48.9 ± 1.5
S13	26.6439	119.8005	29.8	25.9	1.64 ± 0.35	37.6 ± 1.2	23.4 ± 0.6	72.2 ± 1.8
S5	26.6307	119.7519	29.3	27.7	1.02 ± 0.28	37.8 ± 1.3	21.8 ± 0.6	66.4 ± 1.8
S3	26.6181	119.6803	29.1	27.1	2.40 ± 0.22	47.2 ± 1.4	22.9 ± 0.5	76.4 ± 1.9
S10	26.8082	119.6946	29.7	12.6	2.39 ± 0.35	73.8 ± 2.1	26.9 ± 0.7	73.1 ± 2.1
S9	26.7857	119.7049	29.8	14.2	2.10 ± 0.34	73.7 ± 2.1	25.9 ± 0.5	76.3 ± 1.5
S8	26.7381	119.7234	29.8	20.6	1.69 ± 0.27	59.6 ± 1.9	24.8 ± 0.7	77.9 ± 4.2
S11	26.7956	119.7614	30.1	20	2.08 ± 0.29	58.7 ± 1.8	24.4 ± 0.6	75.4 ± 1.6
S12	26.7573	119.7775	30.9	24.8	2.13 ± 0.25	70.1 ± 1.9	26.8 ± 0.7	95.4 ± 2.4
S28	26.6867	119.8201	29.9	26.8	2.17 ± 0.22	53.5 ± 1.7	24.1 ± 0.6	81.8 ± 2.2

[a] If not specified, the samples were collected at surface. In the column of Station "_B" means samples collected at bottom depths and "_*x* m" means sampling depth at *x* m.

to 30.9 at the bay outlet. At stations in the Jiaoxi Stream the temperature was 29.7–29.8 °C and the salinity ranged from 9.6 to 20.6. The stations at the bay outlet, S22–25, had salinities higher in summer than in winter by 0.5–2.2, while at other stations away from the outlet, the salinity was in general lower in summer than in winter by 0.3–3.7 except at stations S2, S5, and S7, where the salinity was higher in summer than in winter by 0.2–0.4 (Table 1). At stations in the Jiaoxi Stream the salinity was the same at Station S8 in both seasons and was lower in summer than in winter by 2.9–5.3 at the other stations. The lower salinity in the bay in summer is due to greater river discharge. The stations at the bay outlet are directly affected by the ECS offshore water, which in winter is lower in salinity due to MCC carrying water from the Yangtze River, so that these stations had salinity lower in winter than in summer. In both seasons the bay water was vertically stratified as shown by density profiles at stations S3 and S26 (Fig. 5). The depth of pycnocline ranged from 2.5 to 40 m in winter and from 1.5 to 10 m in summer.

3.2. Distribution of dissolved radium isotopes in Sansha Bay

The activity of surface dissolved radium isotopes decreased in general from the inner bay to the bay outlet in winter and summer (Figs. 3 and 4) due to mixing with the offshore water that was relatively depleted in radium. Stations with relatively low salinities were usually enriched in radium isotopes, demonstrating the influence of river plumes, except at 3 inner bay stations, S3, S6, and S12, in winter where the activities of the four isotopes had anomalously low values (in dpm 100 L^{-1}), 0.96–1.53 for ^{223}Ra, 13.0–16.7 for ^{224}Ra, 11.5–13.0 for ^{226}Ra, and 37.5–47.2 for ^{228}Ra. These activities are comparable to or even lower than the values near the bay outlet. These stations are

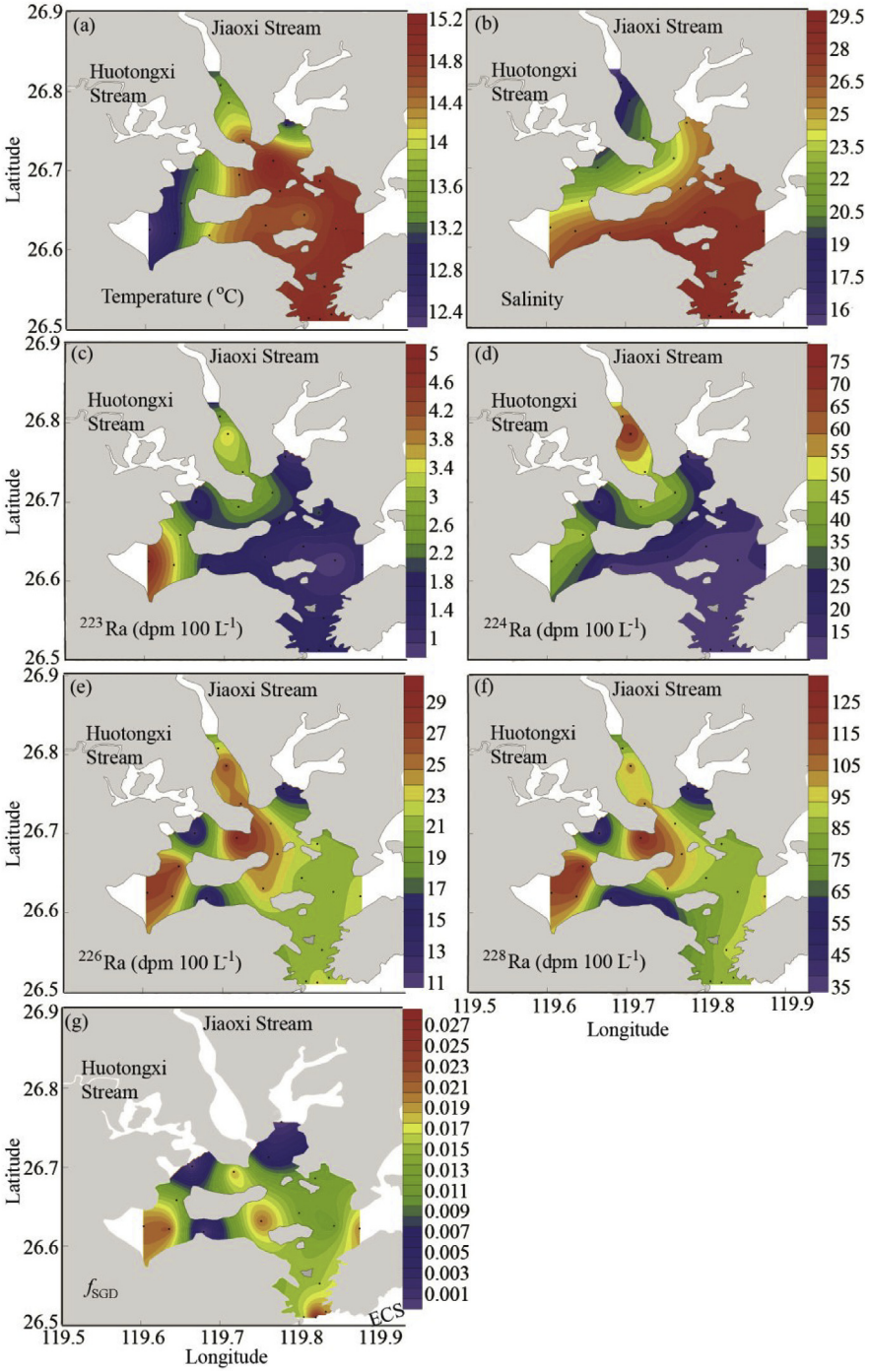

Fig. 3. Surface distributions of temperature, salinity, radium isotopes, and the fraction of SGD (f_{SGD}) in Sansha Bay in Dec. 2013, (a) temperature, (b) salinity, (c) ^{223}Ra, (d) ^{224}Ra, (e) ^{226}Ra, (f) ^{228}Ra, and (g) f_{SGD}. ECS is the East China Sea.

located at either valley or stream inlets and it is inferred that water from these inlets was low in dissolved radium. This difference in the activity of dissolved radium from major river plumes, such as that of the Jiaoxi Stream, is likely caused by very few particles carried by the water from these inlets and consequent little desorption of radium. At other bay stations the activity of ^{223}Ra and ^{224}Ra ranged from 0.84 to 4.93 dpm 100 L^{-1} and from 10.8 to 47.8 dpm 100 L^{-1}, respectively. The range (in dpm 100 L^{-1}) was 21.0–29.5 for ^{226}Ra and 82.7–126.9 for ^{228}Ra. The Jiaoxi Stream stations S8–10 had relatively high activities of short-lived ^{223}Ra and ^{224}Ra, 1.90–3.63 and 51.0–71.7 dpm 100 L^{-1}, respectively and their activities of ^{226}Ra and ^{228}Ra were comparable to those at stations away from the inlets in the bay. In summer the gradual decrease in the activity of dissolved radium from the inner bay to the outlet was apparent without anomalous stations. The range in the activity (in dpm 100 L^{-1}) was 1.02–2.92 for ^{223}Ra, 20.0–76.4 for ^{224}Ra, 14.9–33.6 for ^{226}Ra, and 41.5–95.3 for ^{228}Ra. At the Jiaoxi Stream stations the activities of the four isotopes fell in the range of the activity in the bay.

To evaluate the impact of bottom water, i.e., radium from sediments via diffusion and SGD, on the distribution of radium in the surface water, vertical distributions of radium isotopes were examined at a few stations. The activity of radium at the bottom was up to 50% greater than at the surface for the four isotopes except at Station S26, where the activities of ^{223}Ra and ^{224}Ra were less at the bottom than at the surface

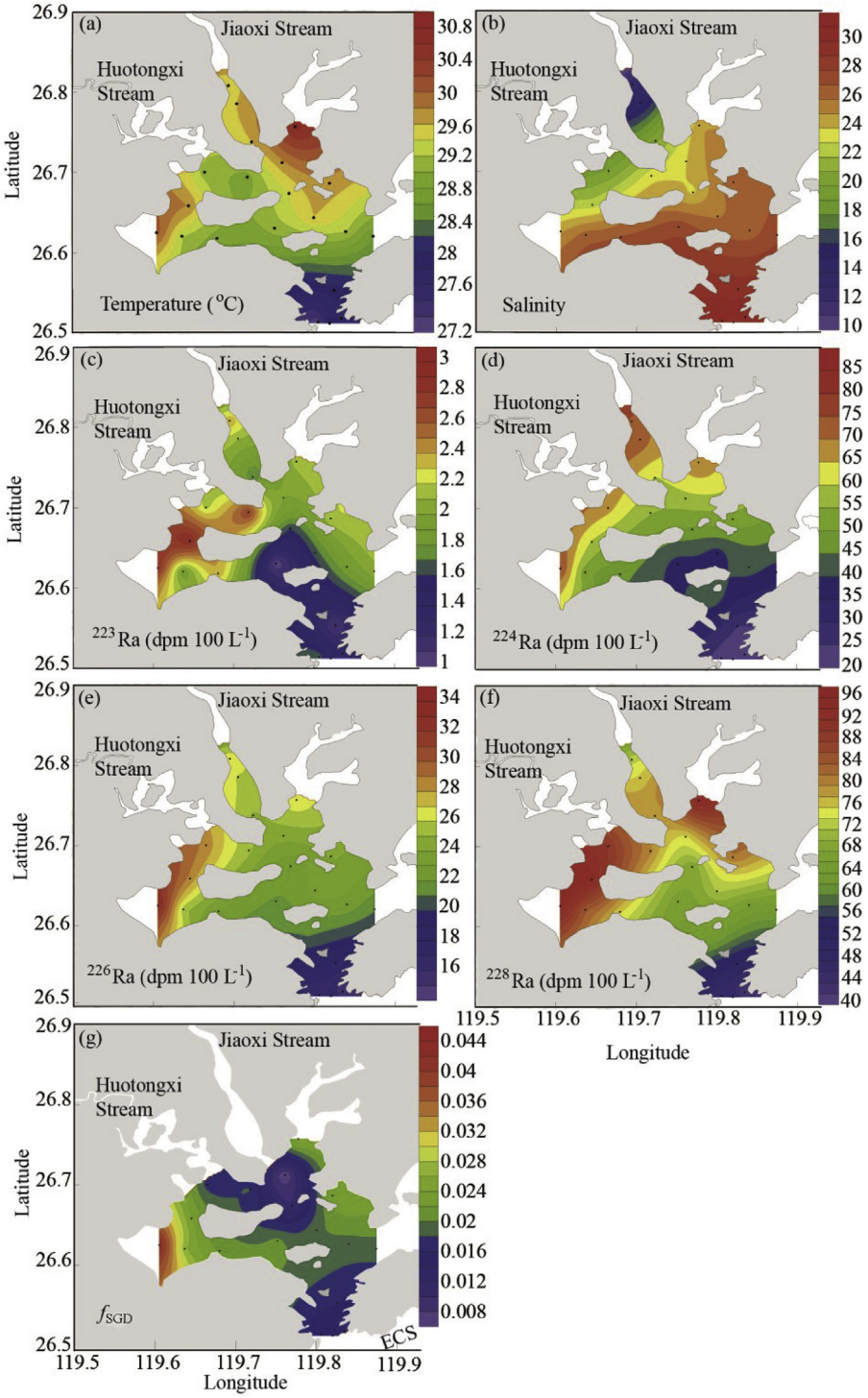

Fig. 4. Surface distributions of temperature, salinity, radium isotopes, and the fraction of SGD (f_{SGD}) in Sansha Bay in Aug. 2014, (a) temperature, (b) salinity, (c) ^{223}Ra, (d) ^{224}Ra, (e) ^{226}Ra, (f) ^{228}Ra, and (g) f_{SGD}. ECS is the East China Sea.

and the activity of ^{228}Ra was almost the same, and Station S14, where the activity of radium decreased with increasing water depth (Fig. 6) and the salinity increased from 26.4 at the surface to 31.1 at the bottom (Table 1). At Station S14 the activity of radium (in dpm 100 L^{-1}) was 1.88 for ^{223}Ra, 42.2 for ^{224}Ra, 22.6 for ^{226}Ra, and 65.8 for ^{228}Ra at the surface and decreased by 10–60% at the bottom. This pattern of lower Ra activity in higher salinity bottom waters may be caused by the intrusion of radium-depleted seawater into the bottom of the bay, which may cap SGD and thus benthic inputs of radium, as in a salt-wedge estuary (Santos et al., 2012). This downward-decreasing trend in radium isotopes confirms that radium from the bottom water imposed little impact on the radium in the surface water in summer.

3.3. Desorbable radium from suspended particles

The activity of particulate ^{224}Ra decreased with increasing salinity from 0.90 ± 0.07 to 0.38 ± 0.10 dpm g^{-1} (Fig. 7). The activity of particulate ^{228}Th was 2.03 ± 0.10 dpm g^{-1} at salinity of 15 and decreased to 1.10 ± 0.08 dpm g^{-1} at salinity of 20. At higher salinities the activity varied in the range of 1.00 ± 0.07–1.36 ± 0.09 dpm g^{-1}

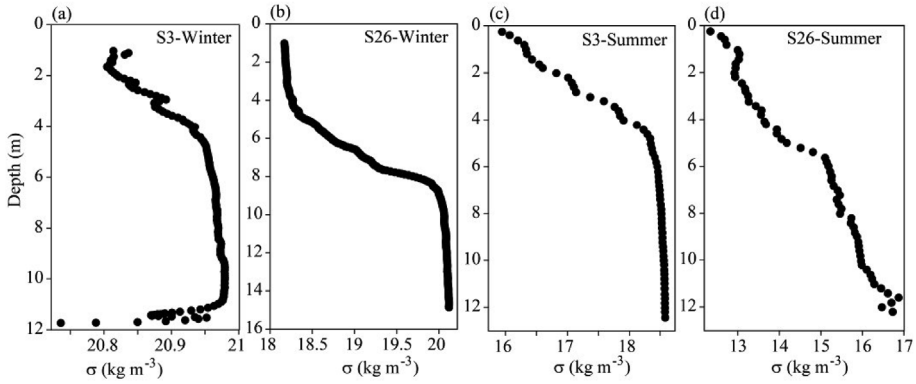

Fig. 5. Vertical profiles of density (σ) at stations S3 and S26 in Sansha Bay in winter (a–b) and summer (c–d).

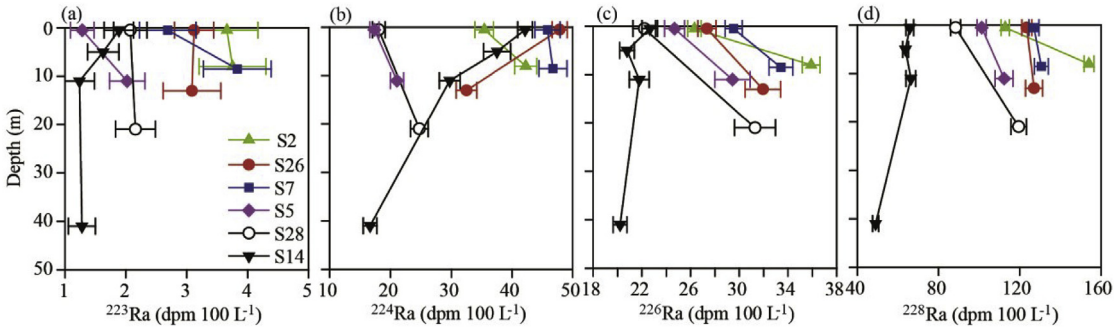

Fig. 6. Vertical profiles of radium isotopes in Sansha Bay, (a) ^{223}Ra, (b) ^{224}Ra, (c) ^{226}Ra, and (d) ^{228}Ra. Station S14 was profiled in summer, while the other stations were sampled in winter.

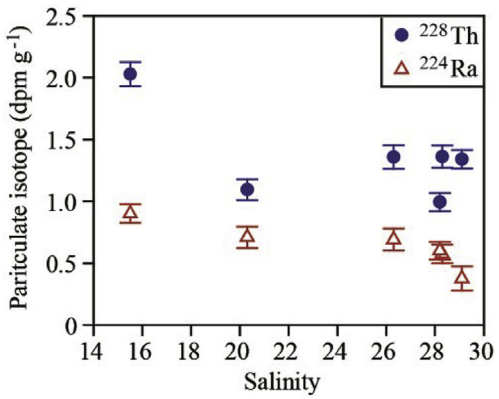

Fig. 7. Activities of particulate ^{228}Th and ^{224}Ra in Sansha Bay.

without a linear trend with salinity. If we assume that ^{224}Ra and ^{228}Th are at equilibrium on suspended particles, the fraction of desorbed ^{224}Ra (f_d) in the bay can be calculated,

$$f_d = 1 - \frac{^{224}Ra_P}{^{228}Th_P} \quad (1)$$

where ^{224}Ra$_P$ is the activity of particulate ^{224}Ra and ^{228}Th$_P$ is the activity of particulate ^{228}Th. The salinity in the bay was at least 20 in both seasons. The fraction of desorbed ^{224}Ra at salinity ≥20 varied from 0.35 to 0.72 with an average of 0.51 ± 0.15, overlapping with the values reported in other coastal regions, e.g., 0.38 on the ECS shelf off the Yangtze River mouth (Gu et al., 2012) and 0.43 in the Jiulong River estuary, China (Wang et al., 2015). The average particulate ^{228}Th was 1.23 ± 0.36 dpm g^{-1}, which makes $^{224}Ra_d$ = 1.23 × 0.51 = 0.63 dpm g^{-1}. The fraction of desorbable ^{226}Ra and ^{228}Ra was assumed to be the same as that of ^{224}Ra. The maximum activity of particulate ^{226}Ra, 2.5 dpm g^{-1}, in other rivers (Krest et al., 1999) was taken to be the activity at equilibrium with its parent nuclide and applied here, which makes $^{226}Ra_d$ = 2.5 × 0.51 = 1.28 dpm g^{-1}.

3.4. Nutrients in the Jiaoxi Stream

In winter the concentration of nutrients at stations S8–10 decreased downstream from 10.1 to 6.1 μM for ammonium, from 1.67 to 1.45 μM for nitrite, from 62.0 to 52.4 μM for nitrate, and from 91.9 to 51.8 μM for silicate. The concentration of phosphate, however, increased downstream from 1.79 to 2.26 μM. In summer the nutrients followed a similar downstream pattern except for nitrite, although the concentration was in general smaller than that in winter. The concentration decreased downstream from 4.31 to 1.39 μM for ammonium, from 36.4 to 26.2 μM for nitrate, and from 105.1 to 61.9 μM for silicate. Phosphate increased downstream from 1.00 to 1.06 μM. Nitrite increased downstream from 2.50 to 3.09 μM. In both seasons nitrate was the dominant species of DIN (≥84%). DIN, phosphate, and silicate were significantly correlated with salinity ($P < 0.05$), negative for DIN and silicate and positive for phosphate (Fig. 8), indicating conservative mixing of these nutrients in the stream.

3.5. Parameters in the groundwater

The salinity at the well sites ranged from 0 to 0.1 in winter and remained the same in summer except at Station GW4 where the salinity was 0.1 in winter and 0.2 in summer. The uncertainty in conductivity measurements is 1%, and the precision of the salinity is 0.1. In winter the activity of radium (in dpm 100 L^{-1}) varied in the range of 1.89–5.56 for ^{223}Ra, 43.1–85.7 for ^{224}Ra, 31.5–46.4 for ^{226}Ra, and 34.0–57.3 for ^{228}Ra at the salinity of 0 and increased by about an order of magnitude at stations where the salinity was 0.1. The concentration of DOC fell in the range of 16.0–139.1 μM. The maximum DOC appeared at Station GW9 where concentrations of phosphate and DIN were the lowest (Table 2). The concentration of DIN at stations with

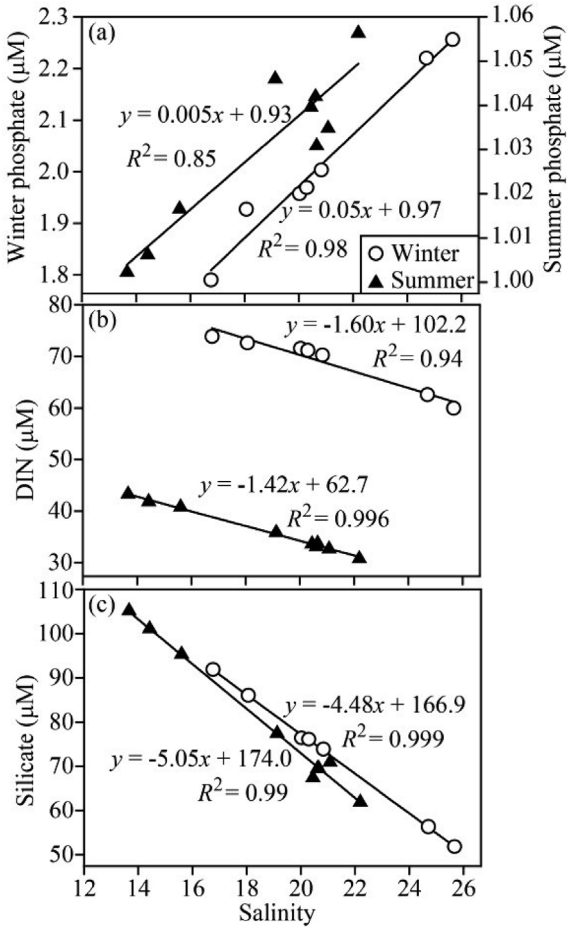

Fig. 8. The nutrient concentrations vs. salinity in the Jiaoxi Stream in winter and summer.

salinity of 0.1 was at least a few times greater than that with salinity of 0. The concentration of nutrients at these stations varied by up to two orders of magnitude for phosphate in the range of 0.37–24.8 μM and DIN in the range of 13.6–1885 μM, and by much less for silicate in the range of 313–620 μM. In summer the activity of radium was close (within 30% difference) to that in winter for ^{224,226,228}Ra at stations where there was no seasonal change in salinity. At Station GW4 where the salinity was 0.2 in summer, the activity (in dpm 100 L^{-1}) almost doubled to 932 for ^{224}Ra, 717 for ^{226}Ra, and 1121 for ^{228}Ra, the maxima at these stations. The activity of ^{223}Ra, however, decreased by about half at all the stations. Concentrations of DOC increased by 87% at Station GW1 and decreased by about 13% at stations GW2 and GW4. There was almost no change of DOC at Station GW3. Nutrients changed without a uniform trend. Phosphate changed to a greater range from below the detection limit (BDL) to 30.58 μM. Silicate increased by about 10% at stations GW1 and GW2, while decreased by nearly 10% at stations GW3 and GW4. DIN increased by 6–76% except at Station GW2 where DIN decreased by 19%. In both seasons the DOC concentration at most groundwater stations was less than that in the ambient surface seawater, which was 108.5 μM at Station E on the East China Sea coast in winter and 92 μM near the Mainland coast in the northern Taiwan Strait in summer (Lin et al., 2016b). However, the relatively low groundwater DOC concentration in Sansha Bay is not unique. In the Longquanwan Bay subterranean estuary in southwest Taiwan, where the groundwater similarly originates from the adjacent mountainous area and is relatively intact, the groundwater DOC mostly fell in the range of 24–73 μM and was lower than the adjacent surface seawater DOC of 90–99 μM (Yang et al., 2015).

The activity ratio of ^{228}Ra to ^{226}Ra varied from 1.43 to 1.69 in summer at all the groundwater stations except stations GW5 and GW6, where the ratio was 0.84 and 2.58, respectively, both of which were further away from our investigation area to the northeast. The ratio ranged from 1.18 to 1.59 in winter, except at Station G8, where the ratio was 0.73, located further northeastward at the coast of ECS. This close proximity to 1.45 in the activity ratio at stations from both seasons (Fig. 9a) implies similar compositions of the source aquifers around the bay except in the northeast region. The relatively high radium activity at a couple of groundwater stations seemed to be related to saltwater intrusion as indicated by relatively high salinity at these stations (Fig. 9b).

4. Discussion

4.1. Apparent water ages in Sansha Bay

Apparent water age derived from short-lived radium distributions is the time elapsed since the water parcel enriched in Ra leaves the source (Moore, 2000a). To utilize this method, one basic assumption to satisfy is that after the water leaves the source, there are no additions or losses of Ra except for mixing and radioactive decay. In Sansha Bay the water column was stratified in winter and summer. The stratification ensured negligible input of radium from sediments in the investigated area of the bay. The distribution of surface salinity was consistent with the

Table 2
Parameters in the groundwater around Sansha Bay. Depth is the water depth in the well. S means salinity and DIP represents phosphate.

Station	Latitude	Longitude	Depth	S	^{223}Ra	^{224}Ra	^{226}Ra	^{228}Ra	DOC	NH_4^+	NO_2^-	NO_3^-	DIP	Silicate
	°N	°E	m		dpm 100 L^{-1}				μM					
Winter (December 2013)														
GW1	26.7600	119.5459	8	0	5.45 ± 0.66	72.0 ± 2.0	34.8 ± 1.1	55.3 ± 2.1	15.96	3.66	0.94	112	0.77	620
GW2	24.2588	118.0813	0.5	0	4.95 ± 0.95	85.7 ± 3.9	37.5 ± 1.0	57.0 ± 1.9	31.04	2.39	0.31	190	0.61	365
GW3	26.6523	119.5880	1.5	0.1	42.7 ± 8.2	404 ± 11	144 ± 3	213 ± 7	43.61	142	1.43	1741	0.52	313
GW4	26.6683	119.5560	3	0.1	73.1 ± 9.3	416 ± 13	555 ± 8	688 ± 15	86.06	2.39	0.84	1763	24.8	453
GW8	26.9296	120.1471	0.5	0	5.56 ± 0.82	46.5 ± 2.1	46.4 ± 1.0	34.0 ± 1.6	19.55	1.23	0.18	247	1.51	552
GW9	26.7281	119.6778	25	0	1.89 ± 0.45	43.1 ± 1.6	31.5 ± 0.9	37.0 ± 1.8	139.1	12.6	0.07	0.92	0.37	431
Summer (August 2014)														
GW1	26.7601	119.5459	5	0	2.72 ± 0.46	69.4 ± 3.9	35.2 ± 1.1	55.8 ± 2.4	29.85	1.87	0.02	122	BDL[a]	668
GW2	26.6988	119.6214	0.5	0	0.59 ± 0.28	60.3 ± 4.1	29.2 ± 0.9	41.8 ± 1.7	26.87	1.09	0.08	154	30.6	411
GW3	26.6550	119.5919	1.5	0.1	11.4 ± 1.1	348 ± 10	145 ± 4	244 ± 8	43.48	10.3	2.79	2190	BDL	296
GW4	26.6756	119.5580	7	0.2	27.1 ± 1.8	932 ± 26	717 ± 13	1121 ± 28	97.90	0.03	0.23	3111	29.6	410
GW5	26.8223	119.0312	7	0	0.85 ± 0.23	22.0 ± 1.8	19.6 ± 0.8	16.4 ± 1.3	161.4	0.20	1.89	1012	62.6	497
GW6	26.7913	119.9916	nd[a]	0.1	1.52 ± 0.72	47.6 ± 2.3	16.7 ± 0.8	42.2 ± 2.0	68.92	0.92	0.02	400	57.9	581
GW7	26.8576	119.8524	8	0	2.72 ± 0.86	83.5 ± 3.0	63.8 ± 1.8	105 ± 4	51.94	0.20	1.42	516	0.33	568

[a] Nd: not determined. BDL: below the detection limit.

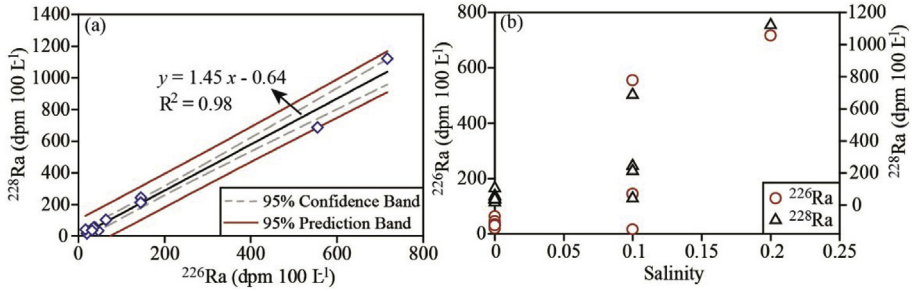

Fig. 9. The activity of ^{228}Ra vs. ^{226}Ra (a) and Ra activity vs. salinity (b) in the groundwater around Sansha Bay.

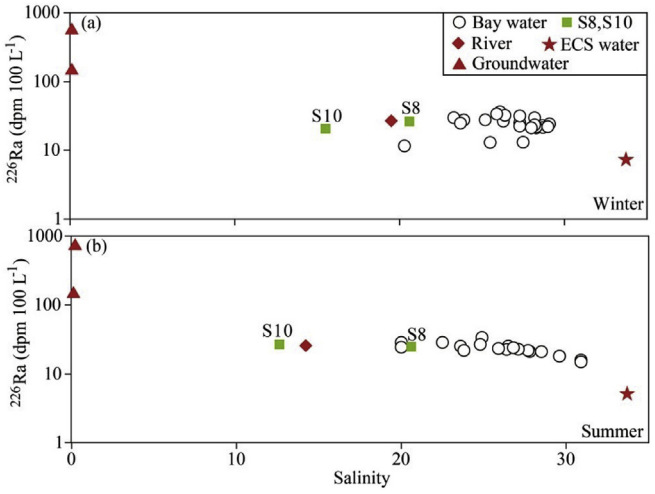

Fig. 10. The activity of ^{226}Ra vs. salinity in the surface water of Sansha Bay, in the groundwater endmember around the bay, and in the Jiaoxi Stream, (a) winter and (b) summer. ECS is the East China Sea.

distribution of surface ^{224}Ra and ^{228}Ra, demonstrating the spread out of the river plumes with relatively high radium activities in the bay. Here, we used excess ^{224}Ra normalized to excess ^{228}Ra to estimate the water age under the assumptions that the activity ratio of the radium source remained constant in each month and that the dispersal of river plumes influenced the distributions of ^{224}Ra and ^{228}Ra. The normalization to long-lived ^{228}Ra was to eliminate the effect of mixing. The equation was expressed as

$$\left[\frac{ex^{224}Ra}{ex^{228}Ra}\right]_{obs} = \left[\frac{ex^{224}Ra}{ex^{228}Ra}\right]_{i} \cdot e^{-\lambda_{224}\cdot\tau} \quad (2)$$

where *ex* represents the measured Ra activity in excess of the value (in dpm 100 L^{-1}) in the offshore ECS surface water (6.07 and 4.73 for ^{224}Ra and 15.7 and 13.3 for ^{228}Ra in winter and summer, respectively (*Wang G.*, unpublished data)), $\left[\frac{ex^{224}Ra}{ex^{228}Ra}\right]_{obs}$ is the activity ratio of the surface water in the bay, $\left[\frac{ex^{224}Ra}{ex^{228}Ra}\right]_{i}$ is the activity ratio of the radium source, λ_{224} is the decay constant of ^{224}Ra, 0.1893 d^{-1}, and τ is the water age of the surface water in the bay. Here, the stream station closest to the bay, S8, was taken as the radium source.

The water age thus determined was 0.2–10.8 days in winter with an average of 5.5 ± 3.6 days and 0.2–3.0 days, except for stations S1 and S11, in summer with an average of 1.5 ± 0.8 days. The relatively high normalized excess ^{224}Ra at stations S1 and S11 was likely due to inputs from the shoreline that were relatively enriched in ^{224}Ra compared to ^{228}Ra. If the two brackish groundwater stations sampled in both seasons were taken to represent SGD endmember and the one with the lower ratio were used as the radium source, a water age greater by 0.83 days would result in winter and there would be almost no change in the water age in summer at each station in the bay.

4.2. Submarine groundwater discharge

Two models were applied here to estimate the flux of SGD with ^{226}Ra selected as a tracer. The first model considers conservative mixing of salinity and ^{226}Ra in the bay. Using this model the fraction of each endmember in the water mass can be determined at each station. The second model assumes steady state of ^{226}Ra in the bay, i.e., the ^{226}Ra sources equal the ^{226}Ra sinks. This model considers the bay as a box and utilizes the average bay values in the calculation. No value can be obtained for each station using the box model. Radioactive decay can be neglected in setting up the mass balance of ^{226}Ra in the bay due to its relatively long half life.

4.2.1. Flux of SGD estimated using a three end-member mixing model

The surface salinity in the bay was no less than 20 (Figs. 3 and 4) and the average concentration of TSM in the bay was 17.8 ± 6.4 mg L^{-1}. ^{226}Ra desorbed from particles was thus calculated with the product of $^{226}Ra_d$, 1.28 dpm g^{-1}, and the concentration of TSM to be 2.28 ± 0.82 dpm 100 L^{-1}. Dissolved ^{226}Ra behaved conservatively in the bay after desorption correction. Salinity and ^{226}Ra were, therefore, chosen to be the conservative tracers for mixing of the water mass in the bay. Based on the activity of ^{226}Ra and salinity in the surface water (Fig. 10), the water above the minimum pycnocline in the bay was potentially contributed by three end-members: rivers, SGD, and the ECS water. The benthic input of ^{226}Ra can be neglected due to stratification of the water column. A three end-member mixing model was thus set up as follows to solve for the fraction of each end-member,

$$\begin{cases} f_O + f_R + f_{SGD} = 1 \\ S_O \cdot f_O + S_R \cdot f_R + S_{SGD} \cdot f_{SGD} = S_B \\ {}^{226}Ra_O \cdot f_O + {}^{226}Ra_R \cdot f_R + {}^{226}Ra_{SGD} \cdot f_{SGD} = {}^{226}Ra_{BC} \end{cases} \quad (3)$$

where *f* is the fraction of each end-member in the bay, *S* is salinity, ^{226}Ra is the activity of dissolved ^{226}Ra, the subscript '$_O$' means the ECS ocean end-member, '$_R$' is the river end-member, '$_{SGD}$' is the SGD end-member, S_B represents bay water salinity, and $^{226}Ra_{BC}$ represents desorption-corrected ^{226}Ra of the bay water. For the groundwater end-member the average of the two brackish stations sampled in both seasons was taken. The stream station S9 was taken as the river end-member. The data collected in ECS (121.4908 °N, 25.8993 °E) was taken as the ocean end-member. All the values for the three end-members were listed in Table 3.

The model results were shown in Figs. 3g, 4g and 11. In winter the fraction of groundwater ranged from 0 to 3% (Figs. 3g and 11), with an average of 1.4 ± 0.8%. The contribution of the river water fell in the range of 26–100%. In summer groundwater contributed 1–4% to the bay water (Figs. 4g and 11), with an average of 2.0 ± 0.8%. The fraction of the river water in the bay spanned from 12 to 69%. The fraction of SGD in the bay water was fairly small compared to the ocean water and river water. This indicates that in terms of water mass in the bay SGD contributed the least.

Table 3
Parameters applied in the three end-member mixing model.

	Parameter		Value	Unit
Groundwater end-member	S_{SGD}	Winter	0.1 ± 0.06	–
		Summer	0.15 ± 0.07	
	$^{226}Ra_{SGD}$	Winter	350 ± 290	dpm 100 L^{-1}
		Summer	431 ± 405	
River end-member	S_R	Winter	19.5 ± 0.04	–
		Summer	14.2 ± 0.04	
	$^{226}Ra_R$	Winter	26.7 ± 0.6	dpm 100 L^{-1}
		Summer	25.9 ± 0.5	
Ocean end-member	S_O	Winter	33.73 ± 0.05	–
		Summer	33.69 ± 0.05	
	$^{226}Ra_O$	Winter	7.29 ± 0.52	dpm 100 L^{-1}
		Summer	5.16 ± 0.22	

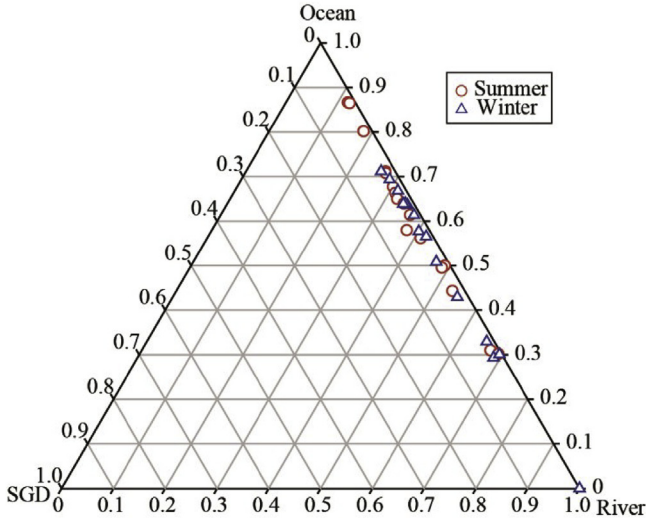

Fig. 11. Ternary plot showing fractions contributed by submarine groundwater discharge (SGD), the East China Sea ocean water, and the rivers in Sansha Bay in winter and summer calculated using a three end-member mixing model based on the conservation of ^{226}Ra and salinity.

With the average fraction of SGD and the average water age in the bay, we estimated the flux of SGD (F_{SGD}) as follows (Liu et al., 2012),

$$F_{SGD} = \frac{V \cdot f_{GW}}{\tau} \quad (4)$$

where V is the water column above the minimum pycnocline in the bay, 3.66×10^8 m^3. The flux of SGD calculated was $9.33 \pm 8.17 \times 10^5$ m^3 d^{-1} in winter and $4.89 \pm 3.35 \times 10^6$ m^3 d^{-1} in summer, about an order of magnitude smaller than the concomitant river discharge of 1.17×10^7 m^3 d^{-1} in winter and 2.65×10^7 m^3 d^{-1} in summer. Similarly, the flux of tidal exchange was calculated to be 3.33×10^7 m^3 d^{-1} in winter and 1.52×10^8 m^3 d^{-1} in summer.

4.2.2. Flux of SGD estimated using a box model

In Sansha Bay the sources of dissolved excess ^{226}Ra include inputs from rivers (including dissolved Ra and desorbed Ra from particles), diffusion from sediments, and SGD. The sink of dissolved ^{226}Ra is the exchange with the ECS water. Under steady state, sources of ^{226}Ra balance the sink of ^{226}Ra. The mass balance approach has been frequently used to quantify SGD (Charette et al., 2008 and references therein). The mass balance of ^{226}Ra was set up for Sansha Bay as

$$F_R \cdot {}^{226}Ra_R + F_R \cdot {}^{226}Ra_d \cdot C_{TSM} + F_{sed} \cdot A + F_{SGD} \cdot {}^{226}Ra_{GW} = \frac{I_{226}}{\tau} \quad (5)$$

where F_R is the total river water discharge, including the Jiaoxi Stream and Huotongxi Stream; $^{226}Ra_R$ is the activity of dissolved ^{226}Ra of the river, here the activity at Station S9 was taken; C_{TSM} is the concentration of TSM; $^{226}Ra_d$ is the activity of desorbed ^{226}Ra from suspended particles; F_{sed} is the diffusion flux of ^{226}Ra from sediments, A is the surface area of our investigation, $^{226}Ra_{GW}$ is the activity of dissolved ^{226}Ra in the groundwater; and I_{226} is the total inventory of dissolved excess ^{226}Ra in the bay above the minimum mixed-layer depth of 1.5 m.

To calculate the total inventory of excess ^{226}Ra in the bay, the investigated area (excluding stream stations S8-10) was divided into 15 equal-sized grids. The total inventory was calculated from integration of the average radium activity inside each grid above the minimum mixed-layer depth,

$$I_{226} = \sum_{i=1}^{15} [({}^{226}Ra_i - {}^{226}Ra_O) \cdot H \cdot A_i] \quad (6)$$

where $^{226}Ra_i$ is the average activity of dissolved ^{226}Ra measured in the ith grid, $^{226}Ra_O$ is the activity of dissolved ^{226}Ra of the offshore ECS water (7.3 and 5.2 dpm 100 L^{-1} in winter and summer, respectively (*Wang G.*, unpublished data)), H is the minimum mixed-layer depth in the bay, 1.5 m, and A_i is the surface area of each grid, 1.63×10^7 m^2.

Based on these calculations the total input of the excess ^{226}Ra to the water column above the minimum pycnocline in the bay was $5.35 \pm 0.08 \times 10^{10}$ and $6.97 \pm 0.06 \times 10^{10}$ dpm d^{-1} in winter and summer, respectively. The activity of ^{226}Ra at the two brackish groundwater stations sampled in both seasons was taken to represent $^{226}Ra_{GW}$. When the parameters in Eq. (5), except F_{SGD}, are known, as listed in Table 4, the flux of SGD can be calculated. Rivers contributed 38% in winter and 17% in summer to the total excess ^{226}Ra in the bay, and the benthic diffusional flux accounted for less than 2% of the total excess ^{226}Ra flux in both seasons, while SGD contributed the rest of the excess ^{226}Ra. The flux of SGD was calculated to be $1.08–4.13 \times 10^6$ m^3 d^{-1} in winter and $0.54–2.67 \times 10^7$ m^3 d^{-1} in summer.

The flux of SGD calculated using the three end-member mixing model was similar to the minimum flux calculated using the box model. However, the SGD flux based on the three end-member mixing model has less uncertainty than that based on the box model. The minimum flux of SGD was a few times smaller than the concomitant river discharge in Sansha Bay in summer and about an order of magnitude smaller than the river discharge in winter. The area-normalized flux of SGD was 0.4 ± 0.3 cm d^{-1} (0.4–1.7 cm d^{-1}) in winter and 2.0 ± 1.4 cm d^{-1} (2.2–10.9 cm d^{-1}) in summer based on the mixing model (the numbers in the parenthesis are based on the box model). Due to hydrologic heterogeneity in the groundwater aquifer in this region (Wu, 2011), however, the SGD seepage rate may actually vary greatly along the tortuous coastline of Sansha Bay. Spatial variability of SGD may likely be driven by onshore topography (Mulligan and Charette, 2016). The majority of meteoric groundwater is rock fissure water in this region, which is overall not abundant due to steep

Table 4
Values of the parameters, except the flux of SGD, in the box model.

Parameter	Season	Value	Unit
$^{226}Ra_R$	Winter	26.7 ± 0.6	dpm 100 L^{-1}
	Summer	25.9 ± 0.5	
$^{226}Ra_{GW}$	Winter	144–555	dpm 100 L^{-1}
	Summer	145–717	
I_{226}	Winter	5.35×10^{10}	dpm
	Summer	6.97×10^{10}	
F_R	Winter	1.17×10^7	m^3 d^{-1}
	Summer	2.65×10^7	
τ	Winter	5.49 ± 3.64	d
	Summer	1.50 ± 0.83	
C_{TSM}	Winter & summer	37.0	mg L^{-1}
$^{226}Ra_d$		1.28	dpm g^{-1}
F_{sed}		0.25	dpm m^{-2} d^{-1}
A		2.439×10^8	m^2

Table 5
SGD fluxes in Asian regions.

Region	Time	SGD flux (10^{-2} m^3 m^{-2} d^{-1})	Aquifer	References
Manila Bay, Philippines	Jan. 2005	0–26	Volcaniclastic sediments	Taniguchi et al., 2008
Bangdu Bay, Korea	Nov. 2008	32.9–49.3	Mainly basaltic lava	Hwang et al., 2005
Bay of Bengal	March 1991	1.1–11.0	Fluvial deposits	Moore, 1997
Jiulong River estuary, China	Jan. 2011	4–8	Holocene deposits	Wang et al., 2015
	July 2010	10–20		
Sansha Bay, China	Dec. 2013	0.5 ± 0.4	Volcanic rock and quaternary deposits	This study
	Aug. 2014	3.0 ± 1.9		

topography and not well-developed fissures (Wu, 2011). In 2014 groundwater supply was 1×10^7 m^3 in this region, accounting for 0.6% of the total water supply (Xiong et al., 2015). To put our results in a regional context, our SGD rates were comparable to some seepage rates in Manila Bay, Philippines where volcaniclastic sediments form the aquifer, while our rates were a few times or even an order of magnitude smaller than in other Asian areas (Table 5). The similarity and difference in the seepage rates in these areas seem to be related to the composition of their aquifers and investigation seasons. Areas with relatively high seepage rates are generally associated with high permeability aquifers, such as Holocene deposits in the Jiulong River estuary, China and basaltic lava in Bangdu Bay, Korea. In these areas summer seems to have relatively high seepage rates than winter.

There are limitations of using Ra as a tracer to estimate the flux of SGD. The activity of Ra in coastal groundwater has been observed to increase with salinity (Cho and Kim, 2016; Mulligan and Charette, 2016). Therefore, the Ra content at the low salinity of the groundwater sampled around Sansha Bay might be much lower than the true Ra content at the discharge interface. If this were the case, the groundwater Ra endmember would have been underestimated and consequently the flux of SGD would have been overestimated. Another limitation of using Ra as a SGD tracer is that fresh groundwater that bypasses the subterranean estuary will not be quantified because fresh groundwater cannot become enriched in Ra without the chance of mixing with more saline groundwater along the interface (Mulligan and Charette, 2016).

4.3. Fluxes of dissolved organic carbon and nutrients via submarine groundwater discharge

To calculate SGD-associated material fluxes, solute concentrations and the activity of ^{226}Ra were plotted together (Fig. 12) to see whether there was any relation between them. There is a pattern that an enrichment in DIN in the groundwater is associated with relatively high activity of ^{226}Ra excluding Station GW5 (Fig. 12a). A similar pattern is present for DOC, excluding stations GW5 and GW9 (Fig. 12d). For phosphate most stations also followed the similar pattern. But the northeast stations GW5 and GW6 had relatively high concentrations of phosphate around 60 μM, while the activity of ^{226}Ra at these two stations was relatively low, about 20 dpm 100 L^{-1} (Fig. 12b). Samples at Station GW9 were collected at an aquifer at least 25 m deep, which is at least a few times deeper than samples in the other groundwater stations (Table 2). So samples at this station might be from a deep aquifer different from the other stations. Stations GW5 and GW6, although similar in sampling depth to the other stations except GW9, also differed from the other stations in terms of the activity ratio of ^{228}Ra to ^{226}Ra and are much further away in the northeast from our investigation area than most of the other groundwater stations. Silicate, however, showed relatively low concentrations at high ^{226}Ra (Fig. 12c). Thus, we considered that the near-surface aquifers surrounding our investigation area were characterized by positive correlations between nutrient concentrations, except silicate, and Ra activity and between DOC concentration and Ra activity and by a negative correlation between silicate concentration and Ra activity. Unfortunately, no samples with ^{226}Ra activity of 200–450 dpm 100 L^{-1} were available for us to derive valid linear correlations between these solutes and ^{226}Ra. Therefore, SGD-associated material fluxes were calculated using the flux of SGD

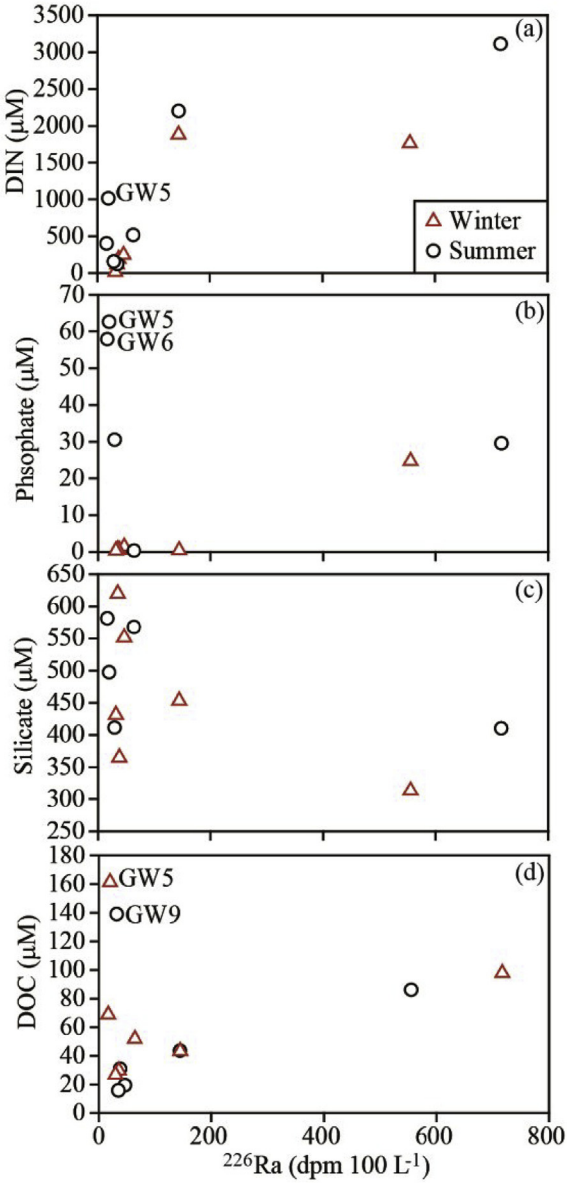

Fig. 12. Concentrations of nutrients and DOC vs. the activity of ^{226}Ra in the groundwater around Sansha Bay, (a) DIN (b) phosphate, (c) silicate, and (d) DOC.

Table 6
SGD-associated material fluxes and the estuarine fluxes (in mol d^{-1}) into Sansha Bay.

Season	Source	DIN	phosphate	Silicate	DOC
Winter	SGD	$1.65–1.76 \times 10^6$	$0.05–2.32 \times 10^4$	$2.92–4.23 \times 10^5$	$4.07–8.03 \times 10^4$
	Streams	1.24×10^6	1.18×10^4	2.02×10^6	–
Summer	SGD	$1.62–2.28 \times 10^7$	$0–2.17 \times 10^5$	$1.45–2.00 \times 10^6$	$3.19–7.18 \times 10^5$
	Streams	1.11×10^6	1.65×10^4	3.09×10^6	–

multiplied by the concentration of the solute in the groundwater end-member stations. The flux of SGD was $9.33 \pm 8.17 \times 10^5\ m^3\ d^{-1}$ in winter and $4.89 \pm 3.35 \times 10^6\ m^3\ d^{-1}$ in summer based on the three end-member mixing model. The concentration of phosphate in summer was 29.58 μM in GW4 and undetectable in GW3, so that the flux of phosphate via SGD into Sansha Bay in summer was calculated to be $0–1.45 \pm 0.99 \times 10^5$ mol d^{-1}. Similarly, the SGD-associated phosphate flux in winter was estimated and listed in Table 6, as well as the flux of DIN, silicate, and DOC via SGD in both seasons.

The estuarine flux of nutrients was estimated using the effective concentration of nutrients multiplied by the river discharge. The effective concentration is the concentration at salinity of 0 for a linear correlation equation between the concentration and mid to high salinity (Office, 1979). From Fig. 8, the effective concentration of phosphate for the Jiaoxi Stream was 0.97 μM in winter and 0.93 μM in summer. The phosphate flux exported from the Jiaoxi Stream was calculated to be 5.77×10^3 mol d^{-1} in winter and 9.88×10^3 mol d^{-1} in summer. Assuming that the Huotongxi Stream had the same effective concentration of nutrients as the Jiaoxi Stream, the total flux of phosphate exported from the Jiaoxi Stream and Huotongxi Stream were estimated to be 1.18×10^4 mol d^{-1} in winter and 1.65×10^4 mol d^{-1} in summer. Similarly, the DIN and silicate fluxes exported from the Jiaoxi Stream and Huotongxi Stream were calculated and listed in Table 6. The estuarine export flux of phosphate was at least two orders of magnitude greater than the minimum SGD-associated flux in both seasons, while the estuarine flux of DIN was comparable to that carried by SGD in winter and an order of magnitude less than the minimum SGD-carried flux in summer. The estuarine export flux of silicate was an order of magnitude greater than that via SGD in winter and about twice as much as the minimum SGD-associated flux in summer.

The annual SGD-carried flux of DIN and phosphate were estimated to be $3.20 \pm 1.81 \times 10^9$–$4.42 \pm 2.55 \times 10^9$ mol and $8.74 \pm 7.65 \times 10^4$–$4.32 \pm 2.43 \times 10^7$ mol. The annual DIN flux via SGD was a few times greater than that from aquaculture and agriculture, which were 6.59×10^8 mol yr^{-1} and 2.20×10^8 mol yr^{-1} (Wang et al., 2011). The phosphate flux via SGD was about twice smaller than that contributed by aquaculture, 6.93×10^7 mol yr^{-1}, reported in Wang et al. (2011), but it was about twice as much as that contributed by agriculture, 1.05×10^7 mol yr^{-1} (Wang et al., 2011).

For comparison with other regions, the material fluxes carried by SGD were divided by the investigated area, $2.44 \times 10^8\ m^2$. SGD-associated phosphate flux in Sansha Bay is similar to that in North Inlet, South Carolina, US, West Neck Bay and Florida Bay in US, and Gulf of Mexico (Krest et al., 2000; Beck et al., 2007; Santos et al., 2008) (Table 7). DIN carried by SGD in Sansha Bay is in the same order of magnitude as the flux in these regions, except Florida Bay, US where the SGD-carried DIN flux is an order of magnitude smaller. The silicate flux via SGD is in the same order of magnitude as that in Gulf of Mexico, but is at least one order of magnitude greater than that in West Neck Bay, US. For SGD-associated DOC flux the values in Sansha Bay are comparable to those in West Neck Bay, New York (Beck et al., 2007). However, they are a few times smaller than the flux in Jeju Island and Masan Bay, Korea (Kim et al., 2013; Oh et al., 2017) or even orders of magnitude less than the flux in Gulf of Mexico, South Carolina, US, Wadden Sea, Germany, and Hat Head, Australia (Goñi and Gardner, 2003; Santos et al., 2008, 2015; Sadat-Noori et al., 2016). The relatively low DOC fluxes in Sansha Bay are associated with the relatively low DOC concentrations in groundwater, which are in general lower than DOC in the ambient surface seawater of the East China Sea coast. The high DOC fluxes in other regions are usually related to the high DOC concentrations in groundwater, which are generally a few times greater than DOC in the ambient surface seawater.

4.4. Implications of SGD for environmental issues

Sansha Bay is a unique embayment in terms of its deep water depth and water stratification in winter and summer. The flux of DIN carried by SGD is comparable to or even greater than the estuarine flux into Sansha Bay, indicating that SGD is a terrestrial N source as important as rivers for Sansha Bay. The production in Sansha Bay was demonstrated to be N limited (Shen et al., 2014). The N:P ratio in the groundwater end-member was greater than 70. SGD, as a main N source for Sansha Bay, apparently helps maintain the production by alleviating N limitation in the bay. Net community production has been demonstrated to be higher at SGD seep sites than adjacent non seeping sites due to phosphate and silicate carried by SGD in the southern Baltic Sea (Donis et al., 2017). SGD has been shown to be directly linked to eutrophication and even harmful blooms in other Asian regions (Hwang et al., 2005; Lee and Kim, 2007; Liu et al., 2017). SGD may contribute to these environmental issues in Sansha Bay. In addition, the unique condition in Sansha Bay makes the bay a natural lab to study hypoxia and regulating mechanisms and processes (including SGD) since the lack of water exchange may induce hypoxia when eutrophication occurs in the bay as shown by observations in the last decade (Cai, 2007; Wang et al., 2014b).

5. Conclusions

Subtropical Sansha Bay is a unique embayment with water stratification in winter and summer and groundwater seeping from the mountains. The flux of SGD into subtropical Sansha Bay, southeastern China was at least a few times smaller than the concomitant major river discharges into the bay. The areal-averaged SGD flux was $3.8 \pm 3.4 \times 10^{-3}\ m^3\ m^{-2}\ d^{-1}$ in winter and $2.0 \pm 1.4 \times 10^{-2}\ m^3\ m^{-2}\ d^{-1}$ in summer. The SGD-associated DIN flux was $1.65–1.76 \times 10^6$ mol d^{-1} in winter and $1.62–2.28 \times 10^7$ mol d^{-1} in summer, comparable to the estuarine flux in winter and was an order of magnitude greater than the estuarine flux in summer. The minimum silicate flux via SGD was 2.92×10^5 mol d^{-1} in winter and 1.45×10^6 mol d^{-1} in summer, which was an order of magnitude less than the estuarine flux in winter and about half as much as the estuarine flux in summer. The phosphate flux exported by the streams was at least two orders of magnitude greater than the minimum flux carried by SGD, which was 0 in summer and 485 mol d^{-1} in winter. The flux of dissolved organic carbon via SGD was $1.67 \pm 1.46 \times 10^{-4}$ – $3.29 \pm 2.88 \times 10^{-4}$ mol $m^{-2}\ d^{-1}$ in winter and $1.31 \pm 0.81 \times 10^{-3}$ – $2.94 \pm 1.81 \times 10^{-3}$ mol $m^{-2}\ d^{-1}$ in summer, which was in the minimum range of the worldwide reported values. Our study indicates that SGD is an important source of nutrients in Sansha Bay. How SGD-associated nutrient and dissolved organic carbon fluxes may contribute to eutrophication and hypoxia in the bay merits further studies.

Table 7
Comparison of SGD-associated material fluxes (in mmol m^{-2} d^{-1}) in Sansha Bay with other regions.

Region	Time	DIN	PO_4	Silicate	DOC	References
Masan Bay, Korea	May	–	–	–	8.4	Oh et al., 2017
	Aug.				7.9	
Hat Head, Australia	March and June	–	–	–	540	Sadat-Noori et al., 2016
Wadden Sea, Germany	Sep.	–	–	–	34–71	Santos et al., 2015
West Neck Bay, New York, US	May	2.4–6.5[a]	$3.7–9.6 \times 10^{-3}$	2.43–5.71 × 10^{-2}	0.6–1.7	Beck et al., 2007
	Oct.	2.4–2.9[a]	$2.9–4.9 \times 10^{-3}$	0–0.14	0.2–0.4	
Hwasun Bay, Jeju Island	Oct.–June	15	–	–	6.7	Kim et al., 2013
Florida Bay, US	Oct.–July	0.30 ± 0.16	0.001 ± 0.0003	–	–	Corbett et al., 1999
North Inlet, South Carolina, US	Annual	2.4[b]	0.9	–	50	Krest et al., 2000; Goñi and Gardner, 2003
Gulf of Mexico	June–Feb.	5.9 ± 0.9	0.35 ± 0.28	5.1 ± 0.2	34 ± 2.8	Santos et al., 2008
Sansha Bay, China	Dec.	6.76 ± 5.92–7.21 ± 6.32	1.99 ± 1.74 × 10^{-3}–0.095 ± 0.083	1.20 ± 1.05–1.74 ± 1.52	0.17 ± 0.15–0.33 ± 0.29	This study
	Aug.	66.2 ± 40.8–93.6 ± 57.7	0–0.89 ± 0.55	5.93 ± 4.06–8.22 ± 5.63	1.31 ± 0.81–2.94 ± 1.81	

[a] Here the flux is for nitrate.
[b] Here the flux is for ammonium.

Acknowledgments and Data

We thank the crew on R/V Minningyu F622 for their assistance in the cruises. Shengyao Sun assisted in the sample collection. We thank the associate editor Isaac Santos and two anonymous reviewers for their constructive comments. The study was funded by MOST (2015CB954001), the National Natural Science Foundation of China (41576074), and the Scientific Research Foundation of Third Institute of Oceanography, State Oceanic Administration, China (2013017). Data can be requested from the first corresponding author.

References

Beck, A.J., Tsukamoto, Y., Tovar-Sanchez, A., Huerta-Diaz, M., Bokuniewicz, H.J., Sañudo-Wilhelmy, S.A., 2007. Importance of geochemical transformations in determining submarine groundwater discharge-derived trace metal and nutrient fluxes. Appl. Geochem. 22 (2), 477–490.

Cai, Q., 2007. Study on marine ecological environment of Sansha bay in Fujian. Environ. Monit. China 23 (6), 101–105.

Cai, W.-J., Wang, Y., Krest, J., Moore, W., 2003. The geochemistry of dissolved inorganic carbon in a surficial groundwater aquifer in North Inlet, South Carolina, and the carbon fluxes to the coastal ocean. Geochem. Cosmochim. Acta 67 (4), 631–639.

Cai, P.H., Shi, X.M., Moore, W.S., Dai, M.H., 2012. Measurement of Ra-224:Th-228 disequilibrium in coastal sediments using a delayed coincidence counter. Mar. Chem. 138, 1–6.

Charette, M.A., Moore, W.S., Burnett, W.C., 2008. Uranium-and thorium-series nuclides as tracers of submarine groundwater discharge. In: Krishnaswami, S., Cochran, J.K. (Eds.), U-Th Series Nuclides in Aquatic Systems. vol. 13. Elsevier, Amsterdam, The Netherlands, pp. 155–191.

Chen, Q., Yan, X., Wang, S., Li, Y., 2014. Characteristics and ecological risk assessment of pollutants in the intertidal surface sediments of Sansha Bay, Fujian. Chin. Trans. Oceanol. Limnol. (2), 37–44. http://dx.doi.org/10.13984/j.cnki.cn37-1141.2014.02.007.

Cho, H.-M., Kim, G., 2016. Determining groundwater Ra endmember values for the estimation of the magnitude of submarine groundwater discharge using Ra isotope tracers. Geophys. Res. Lett. 43, 3865–3871. http://dx.doi.org/10.1002/2016GL068805.

Corbett, D.R., Chanton, J., Burnett, W., Dillon, K., Rutkowski, C., Fourqurean, J.W., 1999. Patterns of groundwater discharge into Florida Bay. Limnol. Oceanogr. 44 (4), 1045–1055.

Donis, D., Janssen, F., Liu, B., Wenzhofer, F., Dellwig, O., Escher, P., Spitzy, A., Bottcher, M.E., 2017. Biogeochemical impact of submarine ground water discharge on coastal surface sands of the southern Baltic Sea. Estuar. Coast Shelf Sci. 189, 131–142.

Du, J., Moore, W.S., Hsh, H.F., Wang, G., Scholten, J., Henderson, P., Men, W., Rengarajan, R., Sha, Z., Jiao, J., 2013. Inter-comparison of radium analysis in coastal sea water of the Asian region. Mar. Chem. 156, 138–145.

Goñi, M.A., Gardner, L.R., 2003. Seasonal dynamics in dissolved organic carbon concentrations in a coastal water-table aquifer at the forest-marsh interface. Aquat. Geochem. 9 (3), 209–232.

Gu, H., Moore, W.S., Zhang, L., Du, J., Zhang, J., 2012. Using radium isotopes to estimate the residence time and the contribution of submarine groundwater discharge (SGD) in the Changjiang effluent plume, East China Sea. Continent. Shelf Res. 35, 95–107.

Huang, D., Ding, G., 2014. Distribution feature and correlation analysis of COD in Sansha Bay. Chin. J. Fujian Fish. 36 (6), 453–458. http://dx.doi.org/10.14012/j.cnki.fjsc.2014.06.006.

Hwang, D.W., Lee, Y.-W., Kim, G., 2005. Large submarine groundwater discharge and benthic eutrophication in Bangdu Bay on volcanic Jeju Island, Korea. Limnol. Oceanogr. 50 (5), 1393–1403.

Kelly, R.P., Moran, S.B., 2002. Seasonal changes in groundwater input to a well-mixed estuary estimated using radium isotopes and implications for coastal nutrient budgets. Limnol. Oceanogr. 47 (6), 1796–1807.

Kim, G., Ryu, J.-W., Yang, H.-S., Yun, S.-T., 2005. Submarine groundwater discharge (SGD) into the Yellow Sea revealed by ^{228}Ra and ^{226}Ra isotopes: implications for global silicate fluxes. Earth Planet Sci. Lett. 237, 156–166.

Kim, G., Kim, J.S., Hwang, D.W., 2011. Submarine groundwater discharge from oceanic islands standing in oligotrophic oceans: implications for global biological production and organic carbon fluxes. Limnol. Oceanogr. 56 (2), 673–682.

Kim, T.H., Kwon, E., Kim, I., Lee, S.A., Kim, G., 2013. Dissolved organic matter in the subterranean estuary of a volcanic island, Jeju: importance of dissolved organic nitrogen fluxes to the ocean. J. Sea Res. 78, 18–24.

Krest, J.M., Moore, W.S., Rama, 1999. ^{226}Ra and ^{228}Ra in the mixing zones of the Mississippi and Atchafalaya Rivers: indicators of groundwater input. Mar. Chem. 64 (3), 129–152.

Krest, J.M., Moore, W.S., Gardner, L.R., Morris, J.T., 2000. Marsh nutrient export supplied by groundwater discharge: evidence from radium measurements. Global Biogeochem. Cycles 14 (1), 167–176.

Lee, Y.-W., Kim, G., 2007. Linking groundwater-borne nutrients and dinoflagellate red-tide outbreaks in the southern sea of Korea using a Ra tracer. Estuar. Coast Shelf Sci. 71 (1–2), 309–317.

Li, F., Zhang, J., Mei, S., Li, N., 2009. The impact of farmland soil loss to water environment in Sansha Bay. Chinese Sci. Technol. Inf. 17, 746–747.

Li, P., Lei, Y., Xie, H., Lu, J., 2014. Water pollution analysis and protection measures of

drinking water sources of Jiaocheng Section of Huotong River. Chin. J. Hengshui Univ. 16 (1), 92–96. http://dx.doi.org/10.3969/j.issn.1673-2065.2014.01.029.
Lin, H., 2014. Tidal characteristics in the Sansha bay of Fujian. J. Fujian Fish. 36 (4), 306–314. http://dx.doi.org/10.14012/j.cnki.fjsc.2014.04.003.
Lin, H., An, B., Chen, Z., Sun, Z., Chen, H., Zhu, J., Huang, L., 2016a. Distribution of summertime and wintertime temperature and salinity in the Sansha Bay. J. Xiamen Univ. 3, 349–356.
Lin, H., Cai, Y., Sun, X., Chen, G., Huang, B., Cheng, H., Chen, M., 2016b. Sources and mixing behavior of chromophoric dissolved organic matter in the Taiwan Strait. Mar. Chem. 187, 43–56.
Liu, Q., Dai, M., Chen, W., Huh, C.-A., Wang, G., Li, Q., Charette, M.A., 2012. How significant is submarine groundwater discharge and its associated dissolved inorganic carbon in a river-dominated shelf system? Biogeosciences 9, 1777–1795.
Liu, Q., Charette, M.A., Henderson, P.B., McCorkle, D.C., Martin, W., Dai, M., 2014. Effect of submarine groundwater discharge on the coastal ocean inorganic carbon cycle. Limnol. Oceanogr. 59 (5), 1529–1554.
Liu, J., Su, N., Wang, X., Du, J., 2017. Submarine groundwater discharge and associated nutrient fluxes into the Southern Yellow Sea: a case study for semi-enclosed and oligotrophic seas-implication for green tide bloom. J. Geophys. Res. Oceans 122. http://dx.doi.org/10.1002/2016JC012282.
McCoy, C., Viso, R., Peterson, R.N., Libes, S., Lewis, B., Ledoux, J., Voulgaris, G., Smith, E., Sanger, D., 2011. Radon as an indicator of limited cross-shelf mixing of submarine groundwater discharge along an open ocean beach in the South Atlantic Bight during observed hypoxia. Continent. Shelf Res. 31 (12), 1306–1317.
Moore, W.S., 1984. Radium isotope measurements using germanium detectors. Nucl. Instrum. Meth. Phys. Res. 223 (2), 407–411.
Moore, W.S., 1997. High fluxes of radium and barium from the mouth of the Ganges-Brahmaputra river during low river discharge suggest a large groundwater source. Earth Planet Sci. Lett. 150 (1–2), 141–150.
Moore, W.S., 2000a. Ages of continental shelf waters determined from ^{223}Ra and ^{224}Ra. J. Geophys. Res.: Oceans (1978–2012) 105 (C9), 22117–22122.
Moore, W.S., 2000b. Determining coastal mixing rates using radium isotopes. Continent. Shelf Res. 20, 1993–2007.
Moore, W.S., 2010. The effect of submarine groundwater discharge on the ocean. Annu. Rev. Mar. Sci. 2, 59–88.
Moore, W.S., Arnold, R., 1996. Measurement of ^{223}Ra and ^{224}Ra in coastal waters using a delayed coincidence counter. J. Geophys. Res. 101 (C1), 1321–1329.
Moore, W.S., Key, R.M., Sarmiento, J.L., 1985. Techniques for precise mapping of 226Ra and 228Ra in the ocean. J. Geophys. Res. 90 (C4), 6983–6994.
Moore, W.S., Blanton, J.O., Joye, S.B., 2006. Estimates of flushing times, submarine groundwater discharge, and nutrient fluxes to Okatee Estuary, South Carolina. J. Geophys. Res. 111http://dx.doi.org/10.1029/2005JC003041. C09006.
Mulligan, A.E., Charette, M.A., 2016. Intercomparison of submarine groundwater discharge estimates from a sandy unconfined aquifer. J. Hydrol. 327, 411–425.
Office, C.B., 1979. Discussion of the behavior of nonconservative dissolved constituents in estuaries. Estuar. Coast Mar. Sci. 9, 91–94.
Oh, Y.H., Lee, Y.W., Park, S.R., Kim, T.H., 2017. Importance of dissolved organic carbon flux through submarine groundwater discharge to the coastal ocean: results from Masan Bay, the southern coast of Korea. J. Mar. Syst. 173, 43–48.
Porubsky, W.P., Weston, N.B., Moore, W.S., Ruppel, C., Joye, S.B., 2014. Dynamics of submarine groundwater discharge and associated fluxes of dissolved nutrients, carbon, and trace gases to the coastal zone (Okatee River estuary, South Carolina). Geochem. Cosmochim. Acta 131, 81–97.
Rocha, C., Wilson, J., Scholten, J., Schubert, M., 2015. Retention and fate of groundwater-borne nitrogen in a coastal bay (Kinvara Bay, Western Ireland) during summer. Biogeochemistry 125 (2), 275–299.
Rodellas, V., Garcia-Orellana, J., Masque, P., Feldman, M., Weinstein, Y., 2015. Submarine groundwater discharge as a major source of nutrients to the Mediterranean Sea. Proc. Natl. Acad. Sci. Unit. States Am. 112, 3926–3930.
Sadat-Noori, M., Maher, D.T., Santos, I.R., 2016. Groundwater discharge as a source of dissolved carbon and greenhouse gases in a subtropical estuary. Estuar. Coast 39, 639–656.
Santos, I.R., Burnett, W.C., Chanton, J., Mwashote, B., Suryaputra, I., Dittmar, T., 2008. Nutrient biogeochemistry in a Gulf of Mexico subterranean estuary and groundwater-derived fluxes to the coastal ocean. Limnol. Oceanogr. 53 (2), 705–718.
Santos, I.R., Glud, R.N., Maher, D., Erler, D., Eyre, B.D., 2011. Diel coral reef acidification driven by porewater advection in permeable carbonate sands, Heron Island, Great Barrier Reef. Geophys. Res. Lett. 38http://dx.doi.org/10.1029/2010GL046053. L03604.
Santos, I.R., Cook, P.L.M., Rogers, L., de Weys, J., Eyre, B.D., 2012. The “salt wedge pump”: convection-driven pore-water exchange as a source of dissolved organic and inorganic carbon and nitrogen to an estuary. Limnol. Oceanogr. 57 (5), 1415–1426.
Santos, I.R., Beck, M., Brumsack, H.J., Maher, D.T., Dittmar, T., Waska, H., Schnetger, B., 2015. Porewater exchange as a driver of carbon dynamics across a terrestrial-marine transect: insights from coupled Rn-222 and pCO_2 observations in the German Wadden Sea. Mar. Chem. 171, 10–20.
Shen, L., Li, C., Wu, X., Gong, L., Hao, S., 2014. Temporal and spatial variation characteristics of inorganic nitrogen and active phosphorus and relations with environmental factors in Sansha Bay of Fujian in summer and winter. Chinese J. Appl. Oceanogr. 33 (4), 553–561.
Stewart, B.T., Santos, I.R., Tait, D.R., Macklin, P.A., Maher, D.T., 2015. Submarine groundwater discharge and associated fluxes of alkalinity and dissolved carbon into Moreton Bay (Australia) estimated via radium isotopes. Mar. Chem. 174, 1–12.
Tait, D.R., Erler, D.V., Santos, I.R., Cyronak, T.J., Morgenstern, U., Eyre, B.D., 2014. The influence of groundwater inputs and age on nutrient dynamics in a coral reef lagoon. Mar. Chem. 166, 36–47.
Taniguchi, M., Burnett, W.C., Dulaiova, H., Siringan, F., Foronda, J., Wattayakorn, G., Rungsupa, S., Kontar, E.A., Ishitobi, T., 2008. Groundwater discharge as an important land-sea pathway into Manila Bay, Philippines. J. Coast Res. 24 (1A), 15–24.
Umezawa, Y., Miyajima, T., Kayanne, H., Koike, I., 2002. Significance of groundwater nitrogen discharge into coral reefs at Ishigaki Island, southwest of Japan. Coral Reefs 21 (4), 346–356.
Verdugo, P., Alldredge, A.L., Azam, F., Kirchman, D.L., Passow, U., Santschi, P.H., 2004. The oceanic gel phase: a bridge in the DOM-POM continuum. Mar. Chem. 92, 67–85.
Wang, C., Sun, Q., Jiang, S., Wang, J.-k., 2011. Evaluation of pollution source of the bays in Fujian province. Procedia Environ. Sci. 10, 685–690.
Wang, G., Jing, W., Wang, S., Xu, Y., Wang, Z., Zhang, Z., Li, Q., Dai, M., 2014a. Coastal acidification induced by tidal-driven submarine groundwater discharge in a coastal coral reef system. Environ. Sci. Technol. 48, 13069–13075.
Wang, H., Wei, S., Yang, Z., Zhang, J., Wang, A., 2014b. Preliminary studies on DO distributions and hypoxia of Sansha Bay of Fujian in summer. Chin. Trans. Oceanol. Limnol. 3, 167–174.
Wang, G., Wang, Z., Zhai, W., Moore, W.S., Li, Q., Yan, X., Qi, D., Jiang, Y., 2015. Net subterranean estuarine export fluxes of dissolved inorganic C, N, P, Si, and total alkalinity into the Jiulong River estuary, China. Geochem. Cosmochim. Acta 149, 103–114.
Wu, S., 2011. Engineering Geologic Conditions and Evaluation for the Coastal Industrial Base of Haixin Ningde Industrial Zone. thesis. China University of Geosciences.
Wu, K., Dai, M., Chen, J., Meng, F., Li, X., Liu, Z., Du, C., Gan, J., 2015. Dissolved organic carbon in the south China Sea and its exchange with the western Pacific ocean. Deep Sea Res. Part II Top. Stud. Oceanogr. 122, 41–51.
Xiong, X., Yu, S., Pan, X., Yang, M., Yu, L., Zhang, Y., Gu, Y., Lin, M., Wang, Q., Lin, J., Cai, P., Lin, H., Lin, X., Lin, Q., Cai, J., Yu, S. (Eds.), 2014. 2013 Fujian Province Water Resources Bulletin, pp. 31.
Xiong, X., Yu, S., Cai, P., Yang, M., Yu, L., Zhang, Y., Gu, Y., Lin, M., Cao, C., Wang, Q., Lin, J., Xu, W., Lin, H., Lin, X., Chen, H., Cai, J., Yu, S. (Eds.), 2015. 2014 Fujian Province Water Resources Bulletin, pp. 31.
Xu, J., Xu, Z., 2013. Seasonal succession of zooplankton in Sansha bay, Fujian. Acta Ecol. Sin. 33 (5), 1413–1424.
Xu, J., Liu, S., Xu, Z., Sun, L., Chen, J., 2014. Response of zooplankton community to changes in water masses in the Sansha Bay. Chin. J. Appl. Environ. Biol. 20 (5), 869–876.
Yan, S., Cao, P., 1997. Mineral characteristics of Sansha Bay and its sediment resources. J. Oceanogr. Taiwan Strait 16 (2), 128–134.
Yan, X., Zhai, W., Hong, H., Li, Y., Guo, W., Huang, X., 2012. Distribution, fluxes and decadal changes of nutrients in the Jiulong River estuary, southwest Taiwan strait. Chin. Sci. Bull. 57 (18), 2307–2318.
Yang, L., Chen, C.-T.A., Hong, H., Chang, Y.-C., Lui, H.-K., 2015. Mixing behavior and bioavailability of dissolved organic matter in two constrasting subterranean estuaries as revealed by fluoresence spectroscopy and parallel factor analysis. Estuar. Coast Shelf Sci. 166, 161–169.
Ye, H., Wang, Y., Cao, B., 2007. Tidal prism of Sansha Bay and its water exchange with the open sea. Chin. J. Hohai Univ. (Natural Sciences) 35 (1), 96–98.
Yu, G., Sun, P., Liu, G., Xu, D., Ding, G., Huang, D., 2014. Diagnostic model construction and example analysis of habitat degradation in enclosed bay: II. spatiotemporal variations in habitat degradation in Sansha Bay. Chin. J. Oceanol. Limnol. 32 (3), 636–644.
Zhu, F., Shi, Z.-z., Ling, X.-w., Xia, Y.-j., Li, Y., Weng, Y.-c., Liu, Y.-x., 2013. Relationship between cage aquaculture and environmental quality in Sansha Bay of Ningde. Mar. Sci. Bull. 32 (2), 171–177.